Circadian regulation of protein turnover and proteome renewal

Authors: Estere Seinkmane[1], Sew Y Peak-Chew[1], Aiwei Zeng[1], Nina M Rzechorzek[1], Andrew D Beale[1], David CS Wong[1], John S O'Neill*[1]

[1]MRC Laboratory of Molecular Biology, Francis Crick Avenue, Cambridge, CB2 0QH

*correspondence to: oneillj@mrc-lmb.cam.ac.uk

ABSTRACT

Although costly to maintain, protein homeostasis is indispensable for normal cellular function and long-term health. In mammalian cells and tissues, daily variation in global protein synthesis has been observed, but its utility and consequences for proteome integrity are not fully understood. Using several different protein labelling strategies, we show that protein degradation varies in-phase with protein synthesis, facilitating rhythms in turnover rather than abundance. This results in daily consolidation of proteome renewal whilst minimising changes in composition. By combining mass spectrometry with pulsed isotopic labelling of nascently synthesised proteins, we gain direct insight into the relationship between protein synthesis and abundance proteome-wide, revealing that coupled rhythms in synthesis and turnover are especially salient to the assembly of macromolecular protein complexes, such as ribosomes, RNA polymerase, and chaperonin complex. Daily turnover and proteasomal degradation rhythms render cells and mice more sensitive to proteotoxic stress at specific times of day, potentially contributing to daily rhythms in the efficacy of proteasomal inhibitors against cancer. Our findings suggest that circadian rhythms function to minimise the bioenergetic cost of protein homeostasis through temporal consolidation of turnover.

Introduction

Protein homeostasis, or proteostasis, refers to the dynamic process of maintaining protein abundance and functionality. It involves regulation of synthesis, folding, localisation and degradation of proteins, such that the appropriate proteins are present within the appropriate concentration range, in the correct compartment, at the right time. Multiple quality control and stress response mechanisms function to preserve proteome integrity over multiple timescales (Wolff *et al*, 2014; Harper & Bennett, 2016) whereas failure of proteostasis networks is strongly associated with impairment of cell function as well as ageing-related pathological states such as neurodegeneration (Labbadia & Morimoto, 2015; Hipp *et al*, 2019). By contrast, priming of proteostatic pathways enhances cellular resistance to proteotoxic stress (Rzechorzek et al., 2015).

Circadian (about daily) regulation orchestrates most aspects of mammalian cellular and organismal physiology to anticipate the differing demands of day and night (Dibner *et al*, 2010; Atger *et al*, 2017). Whilst circadian timing is intrinsic to mammalian cell biology (Welsh *et al*, 2004; Yoo *et al*, 2004), *in vivo,* myriad cellular clocks throughout the body are synchronised with daily environmental cycles by systemic timing cues. For example, daily rhythms of feeding entrain cellular clocks through the insulin signalling pathway to stimulate PERIOD ”clock protein” production *via* activation of mechanistic target of rapamycin complexes (mTORC) (Crosby *et al*, 2019). Daily rhythms of PERIOD and mTORC activity facilitate daily rhythms of gene expression, e.g. at the level of mRNA abundance, in multiple tissues *in vivo* as well as in cultured cells under constant conditions (Ramanathan *et al*, 2018; Feeney *et al*, 2016a; Stangherlin *et al*, 2021b; Mauvoisin *et al*, 2014; Jouffe *et al*, 2013; Sinturel *et al*, 2017; Cao, 2018).

Most models for circadian regulation of mammalian cell function have suggested that daily rhythms in the transcription of ‘clock-controlled genes’ leads to daily rhythms in the abundance, and thus activity, of the encoded protein (Cox & Takahashi, 2019; Zhang *et al*, 2014; Andreani *et al*, 2015). However, recent -omics approaches that measure many thousands of individual transcripts and proteins have revealed multiple discrepancies with this hypothesis, such as poor correlations between mRNA and encoded protein abundance

(Stangherlin et al., 2021a). Moreover, the rather modest extent of daily changes in protein abundance (typically < 20%), and poor reproducibility between independent studies (Janich *et al*, 2015; Mauvoisin *et al*, 2014; Reddy *et al*, 2006; Robles *et al*, 2014; Mauvoisin & Gachon, 2019), suggests that physiological variation in protein abundance is unlikely to account for large daily variations in multiple biological functions observed in tissues and cultured cells. Indeed, daily cycles of protein abundance would appear contrary to the essential requirement for proteostasis maintenance that the major fraction of cellular energy budgets are spent to sustain (Buttgereit & Brand, 1995; Lane & Martin, 2010).

Compelling evidence for physiological daily variation in global rates of protein synthesis cannot be ignored, however (Lipton *et al*, 2015; Feeney *et al*, 2016a; Stangherlin *et al*, 2021b). Such observations are difficult to reconcile with linked observations that, excepting feeding-driven changes in mouse liver, total cellular volume and protein levels show little daily variation (Stangherlin *et al*, 2021b; Hoyle *et al*, 2017; Sinturel *et al*, 2017). To resolve these apparent discrepancies we have proposed that, in non-proliferating cells, daily changes in protein synthesis are accompanied by changes in protein degradation (Stangherlin *et al*, 2021a). This predicts that daily rhythms in protein turnover prevail over rhythms in protein abundance to favour rhythmic proteome renewal over compositional variation. In particular, phase-coherent rhythms in protein synthesis and degradation are predicted to be particularly beneficial for coordinated biogenesis of multiprotein complexes, since assembly requires that individual subunits must be present stoichiometrically at the same time, or else be wastefully degraded (Juszkiewicz & Hegde, 2018; Taggart *et al*, 2020).

Here, we aimed to test these predictions by investigating circadian regulation of global protein synthesis and degradation. In so doing, we utilised bulk pulse-chase labelling and also developed a novel time- and fraction- resolved dynamic proteomics approach that provides the first direct and simultaneous proteome-wide measurements of protein synthesis and abundance. Given its importance in health and disease, we also aimed to investigate the functional consequences of rhythmic proteostasis regulation, revealing time-of-day-dependent differential sensitivity to proteotoxic stress in both cells and mice.

Results

Phase-coherent global rhythms in protein synthesis and degradation

We assessed the evidence for cell-autonomous daily variation in protein turnover in confluent cultures of non-transformed quiescent lung fibroblasts derived from PER2::LUC mice, under constant conditions. Using this cellular model, longitudinal bioluminescence recordings from parallel replicate cultures provide a robust report for the activity of the cell-autonomous daily timekeeping (Yoo *et al*, 2004; Feeney *et al*, 2016b). To measure protein degradation in parallel with synthesis, we first employed a traditional ^{35}S-methionine/cysteine pulse-chase labelling strategy (15/60 min).

For pulse alone, ^{35}S incorporation varied significantly over the circadian cycle (Fig. 1a, b, S1a), consistent with previous reports (Stangherlin *et al*, 2021b; Lipton *et al*, 2015). As expected, ~20% of nascently synthesised proteins had been degraded after 1 hour of chase, representing rapid quality control-associated proteasomal degradation of orphan subunits as well as aberrant translation products due to premature termination and/or protein misfolding (Schubert *et al*, 2000; Wheatley *et al*, 1980; Harper & Bennett, 2016). Importantly, the proportion of degraded protein varied over the circadian cycle, being higher around the same time as increased translation (Fig. 1b). This suggests global rates of protein degradation may be temporally co-ordinated with protein synthesis.

To directly test whether the global rate of proteasomal protein degradation is under circadian control, as suggested previously (Desvergne *et al*, 2016; Ryzhikov *et al*, 2019), we employed biochemical assays for proteasomal activity at discrete biological times over the circadian cycle. Over two days under constant conditions we observed a clear and significant ~24h oscillation in proteasomal trypsin-like and chymotrypsin-like activities of the proteasome, but not caspase-like activity (Fig. 1c).

If global rates of proteasome-mediated protein degradation vary in phase with protein synthesis over the circadian cycle, this would result in circadian organisation of nascent protein turnover. To validate this, we employed puromycin, an antibiotic which is

incorporated into nascent polypeptides by both elongating and stalled ribosomes (Nathans, 1964; Semenkov *et al*, 1992) thus making them amenable to immunodetection (Aviner, 2020; Goodman & Hornberger, 2013; Schmidt *et al*, 2009). Unlike ^{35}S-labelled and other amino acid analogues, puromycin can be added to cell media directly, without the need to remove endogenous amino acids, thereby minimising acute perturbations. Whilst most studies have used puromycin incorporation as a proxy for translation rate, we reasoned that protein degradation should also affect the observed levels of puromycylated peptides, as these peptides are prematurely terminated and are thus identified and degraded rapidly by the ubiquitin-proteasome system (UPS; Liu et al., 2012). By combining acute (30 min) puromycin treatment in cells, with or without proteasomal inhibition using bortezomib (BTZ), we sought to compare the overall level of nascent protein synthesis with the proportion degraded within the same time window, to assess nascent protein turnover (Fig. 1d).

Over two days under constant conditions, puromycin incorporation in the presence of BTZ showed significant circadian variation. In contrast, cells that were treated with puromycin alone showed no such variation, and nor did total cellular protein levels (Fig. 1e, Fig. S1b). This supports the hypothesis that phase-coherent daily rhythms in protein degradation act to compensate for rhythms in translation rate, such that the proportion of degraded peptides vary in synchrony with those that were translated (Fig. 1e).

Protein synthesis is the most energetically expensive process that most cells undertake (Buttgereit & Brand, 1995; Lane & Martin, 2010). *In vivo*, the temporal consolidation of global translation might be expected to confer a fitness advantage by organising this energetically expensive process to coincide with the biological time of greatest (anticipated) nutrient availability. In nocturnal mice, for example, hepatic ribosome biogenesis preferentially occurs at night, during the active/feeding phase (Jouffe *et al*, 2013; Jang *et al*, 2015a; Sinturel *et al*, 2017). To explore the physiological relevance of our cellular observations, we adapted the puromycin ± BTZ labelling strategy *in vivo*, to test the specific prediction that nascent protein turnover is increased during the active phase compared with the rest phase. We observed significantly higher turnover in mouse liver during the night (active/feeding phase, ZT13), compared with the daytime (rest/fasting phase, ZT1) (Fig. 1f). We suggest that both in cells and in mouse liver *in vivo*, the daily variation in nascent protein turnover could be an expected

consequence of imperfect translation, which requires ubiquitous protein quality control mechanisms to shield the proteome from defective, misfolded, or orphaned (excess subunit) proteins.

Proteome-wide investigation of circadian protein synthesis, abundance, and turnover

Beyond protein quality control, we considered how circadian regulation of global protein degradation might interact with rhythmic synthesis to impact proteome composition more broadly. In the simplest scenario, protein abundance would correlate with synthesis rate; however, rhythmic degradation might attenuate variation in the abundance of rhythmically synthesised protein, or alternatively it may generate variation in the abundance of constitutively synthesised proteins. We devised a novel proteome-wide approach to test each of these scenarios.

To simultaneously and directly measure of protein production and abundance over the circadian cycle, we utilised pulsed stable isotopic labelling with amino acids in culture (pSILAC), in combination with state-of-the-art mass spectrometry approaches (TMT-based quantification facilitated by FAIMS-MS3 separation and detection) to allow accurate and multiplexed measurements. Although pSILAC is normally applied continuously and protein harvested at multiple points to measure half-life (Doherty *et al*, 2009; Schwanhäusser *et al*, 2011; Ross *et al*, 2021), here we used a fixed time window for SILAC labelling, that encompassed contiguous windows throughout the circadian cycle, to establish any time-of-day differences (Fig. 2a, b).

We reliably detected heavy peptides for 2528 unique proteins, representing estimates of their synthesis at each time window, and compared this with their total abundance calculated from the sum of heavy and light peptides (Supplementary Table 1; examples in Fig. 2c). The specific number or proportion of rhythmically synthesised and/or abundant proteins is expected to vary with detection method (Mei *et al*, 2021; Hughes *et al*, 2017). We therefore employed several methods, including less stringent RAIN and more stringent ANOVA, to compare the extent of temporal variation in protein synthesis and total abundance (Fig. 2d, e).

Similar to previous studies, abundance of most detected proteins showed no significant variation over the circadian cycle (Fig. 2e), consistent with the long average half-life of mammalian proteins (Mathieson *et al*, 2018; Schwanhäusser *et al*, 2011). Amongst those with significant temporal variation, we found that similar proportions of the proteome showed rhythms in synthesis as rhythms in abundance (Fig 2e). Of the rhythmically abundant proteins, a minority showed accompanying rhythms in synthesis, with no difference in phase (Fig. 2e, f). The behaviour of these few proteins aligns with the canonical "clock-controlled gene" paradigm. Strikingly however, the overwhelming majority of rhythmically synthesised proteins showed no accompanying rhythm in abundance and vice versa, i.e., most rhythmically abundant proteins showed no accompanying rhythm in synthesis (Fig. 2e, g). Moreover, the extent of daily synthesis variation was significantly greater than abundance (Fig. 2d). These observations are consistent with widespread rhythmic regulation of protein degradation.

Considering all detected proteins that were either rhythmically synthesised or rhythmically abundant, neither set clustered to a single phase of the circadian cycle (Fig. 2g). Moreover, gene ontology analysis did not reveal functional enrichment for any particular biological process or compartment in either group compared with background.

Targeted investigation of circadian protein synthesis, abundance, and turnover

The experiment above was designed to combine and compare two time-resolved processes —that of circadian variation and that of protein production—and so only considered proteins with reliably detectable heavy label incorporation within a given labelling window (6h) across all timepoints. This inevitably limited and biased the proteome coverage towards abundant proteins with higher synthesis rates, possibly explaining the absence of functional enrichment among rhythmic proteins that have been observed in other studies, as well as the lower level of overall variation in synthesis than would be expected from the bulk labelling investigations.

We therefore sought to refine our method, to gain more insight into the dynamics of circadian proteomic flux, in three ways. First, we employed a shorter pulse (90 min) in order to increase sensitivity to circadian differences, especially those occurring among most recently

synthesised proteins. Second, we added a so-called booster channel, consisting of a fully heavy-labelled cell sample within the TMT mixture, that allows an increase in detection of proteins with lower turnover due to the overall increase in heavy peptide signal. Third, we fractionated cell lysates to enrich for cellular components of interest in order to explicitly test the hypothesis that circadian translational control facilitates the coordinated assembly of multiprotein complexes (Taggart *et al*, 2020; Stangherlin *et al*, 2021a; O'Neill *et al*, 2020). We therefore focused on the macromolecular complex (MMC) fraction that was isolated by gentle cell lysis followed by sequential ultracentrifugation, based on the LOPIT-DC protocol (Geladaki *et al*, 2019). With this new design, heavy peptides within the enriched fraction were quantified across two days (similarly to the first pSILAC experiment), representing proteins synthesised within 1.5h at each timepoint (Fig. 3a, b, Supplementary Table 2). There was a significant circadian variation among the overall amount of heavy labelled peptides that was consistent with rhythmic production of nascent proteins, whereas the total protein level in this fraction showed no change over time (Fig. S2a, b).

Using boosted fractionated pSILAC, we immediately noticed a 3-fold increase in the proportion of proteins that varied significantly over time in their synthesis as compared to the whole-cell level, regardless of algorithm used (Fig. 3c). The production of rhythmically synthesised proteins in this fraction also varied over time to a far greater extent than did their abundance (~2-fold greater variation, Fig. 3d). Moreover, we found that a much higher proportion of detected proteins exhibited rhythms in both synthesis and total abundance than was observed at the whole-cell level (Fig. 3e). Also as in whole-cell, the proportion of proteins showing rhythmic synthesis but not abundance and *vice versa*, was much greater than expected by chance ($p<0.0001$, Fisher's Exact Test). By inference therefore, the proportion of proteins that are rhythmically degraded in this fraction must equal or exceed the proportion that are rhythmically synthesised.

Analysis of the proteins in this fraction revealed 243 annotated multiprotein complexes (from CORUM, COMPLEAT and manual annotation (Ori *et al*, 2016; Giurgiu *et al*, 2019)) to be present, including 82 complexes for which half or more annotated subunits were detected (Supplementary Table 3). It has previously been shown that protein subunits within the same complex tend to share similar turnover rates, which is thought to facilitate their co-ordinated

assembly and removal (Price *et al*, 2010; Mathieson *et al*, 2018). We observed this in our data (Fig. S2c) but can also add a temporal dimension: for complexes such as ribosomes, RNA polymerase, chaperonin (CCT) complex and others, the majority of component subunits not only showed similar average heavy to total protein ratios but also a similar change in synthesis over the daily cycle (Fig. 3f, S2d). This supports the hypothesis that the assembly and turnover of macromolecular protein complexes is under circadian control.

Using an alternative approach to estimate the importance of rhythmicity for interactions of proteins within complexes, we took advantage of the STRING protein-protein interaction database (Szklarczyk *et al*, 2021). Unlike proteins with rhythmic synthesis at the whole-cell level, rhythmic proteins in this complex fraction had significantly more annotated physical interactions than would have been expected by chance given all proteins detected (Fig. 3g, Fig. S3). Importantly, these rhythmically synthesised protein subunits were almost all clustered within the same circadian phase (see Figure 4, discussed below).

To validate these observations by an orthogonal method, under similar conditions (Fig. 3a), we pulse-labelled cells with methionine analogue L-azidohomoalanine (AHA) and analysed incorporation into highest molecular weight protein species detected under native-PAGE conditions (Fig. 3h, S3e). We observed a high-amplitude daily rhythm of AHA incorporation, indicating the rhythmic translation and assembly of nascent protein complexes. Taken together, these results show that daily rhythms in synthesis and degradation may be particularly pertinent for subunits of macromolecular protein complexes.

Temporal consolidation of biological functions

Within the MMC fraction, we found that the vast majority of rhythmically synthesised proteins showed highest synthesis at the same biological time. Gene ontology analysis of these proteins (compared with background of all proteins detected in this fraction) revealed a clear enrichment for RNA binding proteins and terms associated with ribosome assembly (Fig. 4a). At the same circadian phase, rhythmically abundant proteins were similarly enriched for terms relating to RNA binding and ribonucleoprotein biogenesis, as well as many proteins associated with stress granule assembly, such as ataxin-2 and many DDX family members (Fig.

4a,b). Ribosomes and stress granules themselves control protein synthesis and regulate each other, so it is challenging to ascribe causal relationships between the two (Buchan & Parker, 2009; Riggs *et al*, 2020; Delarue *et al*, 2018). Proteins belonging to these classes did not exhibit commensurate total abundance oscillations at the whole-cell level (Fig. 2, Fig. 4b), and this might indicate that some variation in the MMC fraction arises from redistribution between lighter and denser fractions over the circadian cycle, consistent with circadian regulation of protein solubility and compartmentalisation described previously (Wang *et al*, 2019; Stangherlin *et al*, 2021b; Jang *et al*, 2015b; Malcolm *et al*, 2019). Supporting this possibility, we noted a smaller group of rhythmically abundant proteins in the phase preceding ribosome biogenesis, without any accompanying change in synthesis. These proteins were heavily enriched for components and regulators of the actin cytoskeleton ($q<0.05$, Fig. 4c), and entirely consistent with circadian regulation of cytoskeletal dynamics and actin polymeric state that we have described in previous work (Hoyle *et al*, 2017).

Rhythmic response to proteotoxic stress in cells and in mice

Evidently, global protein translation, degradation and complex assembly are crucial processes for cellular proteostasis in general, so cyclic variation in these processes would be expected to have consequences beyond circadian regulation. Elevated levels of misfolded, unfolded, or aggregation-prone proteins perturb proteostasis and provoke proteotoxic stress responses that disrupt cellular function, leading to cell death unless resolved (Santiago *et al*, 2020; Deshaies, 2014). Informed by our observations above (Fig. 1, 3, 4), we predicted that circadian rhythms of global protein turnover would render cells differentially sensitive to perturbation of proteostasis induced by proteasomal inhibition using small molecules such as MG132 and BTZ.

We first assessed the phosphorylation status of eIF2α, the primary mediator of the integrated stress response (ISR) pathway, throughout a full circadian timecourse in fibroblasts under unperturbed versus stress-induced conditions. As expected, acute proteasomal inhibition by 4h treatment with MG132 induced eIF2α phosphorylation to increase overall (Jiang & Wek, 2005), but importantly this induction varied depending on time of drug treatment (Fig. 5b, S4a), with highest fold-change increase observed around the predicted peak of protein

turnover. Phosphorylation of eIF2α leads to inhibition of canonical translation, and was suggested to drive a daily decrease in bulk protein synthesis *in vivo* (Karki *et al*, 2020; Wang *et al*, 2019; Pathak *et al*, 2019). We did not observe any cell-autonomous rhythm in eIF2α phosphorylation under basal conditions (Fig. S4b), and so conclude that daily rhythms *in vivo* likely arise through daily cycles of systemic cues, e.g., feeding and temperature rhythms.

A major detrimental consequence of proteotoxic stress is formation of insoluble intracellular protein aggregates (Albornoz *et al*, 2019; Dantuma & Lindsten, 2010). To test whether this was also time-of-day dependent, we used a molecular rotor dye that becomes fluorescent upon intercalation into quaternary structures associated with protein aggregates (Shen *et al*, 2011) (Fig. S4c). As predicted, over two days, challenging cells with MG132 around the peak of protein turnover resulted in significantly more protein aggregation compared to controls than the same challenge delivered 12 h later (Fig. 5c, S4d).

Sustained proteotoxic stress results in cell death (Santiago *et al*, 2020; Deshaies, 2014), and cell death induced by 6h treatment with BTZ showed a clear circadian rhythm (Fig. 5d). Strikingly, we found roughly twice as much cell death occurred for proteasomal inhibition at the peak of protein turnover compared with its nadir (Fig. 5d, S4e). In contrast, translational inhibition with cycloheximide revealed no such temporal variation. Together, these data support our predictions, wherein proteasomal inhibition at peak times of translation and protein turnover exacerbates proteotoxic stress, protein aggregation, and cell death because the burden on protein quality control systems at these circadian phases is already high.

BTZ and its derivatives are used clinically to treat several types of blood cancers, associated with a multitude of side effects due to the proteasome's essential function in all cells (Deshaies, 2014; Manasanch & Orlowski, 2017; Zhang *et al*, 2020). In light of the daily variation in protein turnover we observed in mouse liver (Fig 1f), we hypothesised that time-of-day sensitivity to BTZ would also be observed *in vivo*. Accordingly, we observed a stark day vs night difference in the response to BTZ treatment in mouse liver, assessed by eIF2α phosphorylation (Fig. 5e, Fig. S4f). Consistent with this, time-of-day variation in BTZ-mediated inhibition of tumour growth was recently demonstrated in a mouse tumour model study (Wagner *et al*, 2021).

Discussion

In this work, we found evidence for coordinated circadian regulation of protein synthesis and degradation, resulting in rhythmic protein turnover. Just as temporal consolidation of protein synthesis is thought to increase its metabolic efficiency (O'Neill *et al*, 2020), we suggest that rhythmic turnover may serve to increase the efficiency of proteostasis by minimising deleterious changes in total cellular protein content and proteome composition.

Increase in translation is inevitably associated with increased production of defective translation products, such as prematurely terminated or misfolded peptides that must be rapidly cleared by UPS-mediated degradation (Dimitrova *et al*, 2009; Wang *et al*, 2013; Gandin & Topisirovic, 2014). Accordingly, we find cell-autonomous circadian rhythms of proteasome activity. More broadly, rhythmic turnover is expected to facilitate daily changes in proteome renewal. Using proteome-wide approaches, we indeed find that a greater proportion of the proteome shows a rhythm in synthesis and/or degradation than a rhythm in protein abundance. Fractionated pSILAC revealed temporal coordination in the synthesis of heteromeric protein complexes. This highlights how, even though most mammalian proteins exhibit half-lives >24h and show little daily variation in abundance, the rate at which they are replaced can be subject to circadian regulation. This may be particularly beneficial for heteromeric complex assembly. Within the MMC fraction, we observed enrichment for specific biological functions at different times of the day, e.g., ribonucleoprotein assembly vs actin polymerisation. While bulk measurements showed clear coordination on the global scale, data from whole-cell and fractionated proteomics suggest that a combination of rhythmic synthesis, degradation, and sequestration acts in concert to temporally organise rhythmic biogenesis whilst minimising changes in overall proteome composition.

More insight into the relationship between temporal organisation and proteostasis can be gained by comparing our findings with other model systems. For example, we recently found chronic proteostasis imbalance in Cry1/2-deficient cells and tissues, that lack circadian transcriptional regulation. These cells exhibit increased proteotoxic stress as well as increased circadian variation in proteome composition compared with wild-type controls (Wong *et al*, 2022). Moreover, the temporal compartmentalisation of proteome renewal processes has a

clear precedent in yeast, where metabolic oscillations arise as a direct consequence of TORC-dependent cycles of protein synthesis and sequestration that are critical for preventing deleterious protein aggregation (O'Neill *et al*, 2020). In light of similar findings in the alga *Ostreococcus tauri* (Kay *et al*, 2021; Feeney *et al*, 2016a), we speculate that promoting and minimising the energetic cost of proteostasis may be an evolutionarily conserved function of circadian and related biological rhythms.

The mechanistic underpinnings for cell-autonomous circadian regulation of the translation and degradation machineries remain to be fully explored, but are likely to involve daily rhythms in the activity of mTORC: a key regulator of protein synthesis, as well as degradation and sequestration (Stangherlin *et al*, 2021a, 2021b; Cao, 2018; Adegoke *et al*, 2019; Ben-Sahra & Manning, 2017; Delarue *et al*, 2018). Given our focus on proteomic flux and translation-associated protein quality control, autophagy was not within the direct scope of this study but is also mTORC-regulated and subject to daily regulation (Ma et al., 2011; Ryzhikov et al., 2019). The daily regulation of mTORC, protein sequestration and proteasomal vs autophagic protein degradation will be a fruitful avenue for future work.

Beyond testing two key predictions in mouse liver, a limitation is that this study was restricted to quiescent primary mouse fibroblasts. In our experience, fibroblasts are a particularly powerful and predictive model for fundamental principles of cellular circadian regulation (Hoyle *et al*, 2017). Clearly though, in future it will be necessary to explicitly validate our expectation that daily rhythms of protein turnover and proteome renewal occur *in vivo* under natural conditions (daily light/dark, feed/fast, rest/activity cycles). We predict that they will be observed across multiple mature tissues, with higher amplitude than cells due to amplification of cell-intrinsic processes by daily systemic cues (hormonal and body temperature rhythms). We anticipate that the relative phases of synthesis and degradation rhythms will likely differ somewhat between tissues and physiological contexts, as recently found in growing muscle for example (Kelu et al, 2020).

Rhythms in transcription were not addressed in this study, but as discussed above, there is a well-established discrepancy between identities and phases of rhythmic proteins and their underlying transcript levels. Regulation at the translational level has been suggested to

explain these differences, although ribosomal profiling studies have noted that on average there appears to be no delay between rhythmic transcript and nascent translation (Atger *et al*, 2015; Janich *et al*, 2015; Jang *et al*, 2015b). We note, however, that ribosomal profiling reports on the level and position of ribosome-mRNA association, and so does not directly measure nascent protein production. Although a good correlate when comparing steady-state conditions, ribosome profiling also does not distinguish between active and stalled ribosomes, and does not reflect all the changes in protein synthesis that occur in dynamic cellular systems or upon perturbation that globally alter proteostasis (Liu *et al*, 2017). Upon finding evidence for global changes in protein synthesis and degradation throughout the day, the development of our pulsed SILAC method was crucial for allowing us direct insight into the regulation of protein abundance. Enabled by technological improvements in peptide detection accuracy and multiplexing, this is the first report of proteins tracked both across their lifetime (production) and across the circadian cycle.

Finally, given the extensive links between proteome imbalance and many pathological states, daily regulation of protein metabolism has implications for health and disease. Circadian disruption is already strongly associated with impaired proteostasis, though causal mechanisms are poorly understood at this time (Bolitho *et al*, 2014; Musiek *et al*, 2018; Leng *et al*, 2019; Lipton *et al*, 2017; Wong *et al*, 2022). In this study we predicted and validated that daily turnover rhythms confer daily variation on the sensitivity of cells and tissues to a clinically relevant proteasome inhibitor. This highlights how preclinical models may help to accelerate the development of (chrono)therapies, that optimise treatment outcomes by leveraging understanding of the body's innate daily rhythms (Cederroth *et al*, 2019).

Methods

Cell culture and general timecourse structure

Fibroblasts originated from mice homozygous for PER2::LUCIFERASE (Yoo *et al*, 2004), isolated from lung tissue and were immortalised by serial passaging as described previously (Seluanov *et al*, 2010). For routine culture, cells were maintained at 37°C and 5% CO_2 in Gibco™ high glucose Dulbecco's Modified Eagle Medium (DMEM), supplemented with 100 units/ml penicillin and 100 µg/ml streptomycin, as well as 10% Hyclone™ III FetalClone™ bovine serum (GE Healthcare). When plated for experiments, cells were grown to confluence prior to the start of assaying, which ensures contact inhibition and elimination of cell division effects during the experiments (Hoyle *et al*, 2017; Ribatti, 2017).

For all the timecourse experiments, cells were subject to temperature entrainment, consisting of 12h:12h cycles of 32°C:37°C, for at least 4 days prior to the start of assaying, with media changes if required. Unless stated otherwise, the final medium change, containing 10% serum, occurred at the anticipated transition from 37°C to 32°C, as the cells were transferred to constant 37°C. This is denoted as experimental time t=0, or start of constant conditions. Sampling began at least 24h afterwards (i.e. t=24+), to avoid any transient effects of the last serum-containing medium change and temperature shift (Balsalobre *et al*, 1998; Buhr *et al*, 2010). A parallel recording of PER2::LUCIFERASE activity was usually obtained using ALLIGATOR (Cairn Research) (Crosby *et al*, 2017), and luminescence quantified in Fiji/ImageJ v2.0 (Abramoff *et al*, 2004; Schindelin *et al*, 2012).

Cell lysis and protein quantification

For timecourse experiments requiring cell lysate collections, the procedure was based on the following. Cells were washed twice with PBS, and incubated with the indicated lysis buffers: normally either digitonin buffer (0.01% digitonin, 50 mM Tris pH 7.4, 5 mM EDTA, 150 mM NaCl) for 10 min on ice or urea/thiourea buffer for 20 min at room temperature (7 M urea, 2 M thiourea, 1% sodium deoxycholate, 20 mM Tris, 5 mM TCEP), both supplemented with protease and phosphatase inhibitor tablets (Roche, 4906845001 and 04693159001) added shortly beforehand. Cells were then scraped, and lysates transferred to Eppendorf tubes, before sonication with Bioruptor sonicator (Diagenode) at 4°C, for 2-3 cycles 30 s on/30 s off.

Lysates were then centrifuged at 14000 rpm for 5 min, and supernatant either flash frozen in liquid nitrogen for future use, or taken directly for further analysis. For determination of protein concentration, Pierce bicinchoninic acid assay (BCA) (Smith *et al*, 1985) was performed in microplate format according to manufacturer's instructions, with bovine serum albumin (BSA) protein standards diluted in the same lysis buffer as experimental samples. Pierce 660 nm assay was performed instead of BCA when samples contained thiourea.

^{35}S pulse-chase labelling

All procedures for ^{35}S pulse-chase were optimised to avoid methionine starvation, serum-containing media changes, and temperature perturbations, all of which could potentially reset circadian rhythms and obscure any cell-autonomous regulation. Fibroblasts were adapted to serum-free but otherwise complete medium starting from the last 4 days of temperature entrainment. At each timepoint, the cells were pulsed with 0.1 mCi/ml ^{35}S-L-methionine and ^{35}S-L-cysteine mix (EasyTag™ EXPRESS35S Protein Labeling Mix, Perkin Elmer) in methionine- and cysteine-free DMEM for 15 min. For chase, the radiolabel-containing media were replaced with standard DMEM supplemented with 2 mM (10x normal concentration) of non-radiolabelled methionine and cysteine, and cells incubated for 1h. Throughout both pulse and chase the cells were maintained at 37°C. At the end of pulse and chase periods, cells were washed with ice-cold PBS and lysed in digitonin buffer (0.01% digitonin (Invitrogen), 50 mM Tris pH 7.4, 5 mM EDTA, 150 mM NaCl for 10 min on ice). Lysates were run on NuPage™ Novex™ 4-12% Bis-Tris protein gels; the gels were then stained with Coomassie SimplyBlue™ SafeStain (ThermoFisher). Gels were then dried at 80°C for 45 min and exposed overnight to a storage phosphor screen (GE Healthcare, BAS-IP SR 2025), which was subsequently imaged with Typhoon FLA700 gel scanner and quantified in Fiji/ImageJ.

Puromycin labelling

Puromycin dihydrochloride, diluted in PBS, alone or in combination with BTZ, was added directly to cells in culture medium, as 10x bolus to a final concentration of 1 µg/ml puromycin and 1 µM BTZ. Labelling proceeded for 30 min at 37°C, after which cells were lysed in a urea/thiourea buffer and puromycin detected by Western blotting.

AHA incorporation

At each timepoint, while still maintaining cells at 37°C, complete DMEM medium was replaced with methionine-free DMEM supplemented with AHA in combination with methionine at 30:1 ratio (Bagert *et al*, 2014) – 1 mM AHA, 33 µM Met - and 1% dialysed FBS for 90 min. Cells were lysed in digitonin buffer (HEPES rather than Tris-buffered). AHA-containing proteins were conjugated to biotin by click chemistry, by adding appropriate reagents (Jena Bioscience) to the lysates, to final concentrations of 1 mM THPTA, 1 mM $CuSO_4$, 2 mM Na ascorbate, and 40 µM biotin alkyne, and incubating for 1h at room temperature. Biotinylated proteins were then detected by Western blotting.

Western blotting

Samples for denaturing polyacrylamide gel electrophoresis (SDS-PAGE) were prepared by diluting lysates with reduced NuPage™ LDS sample buffer and heating at 70°C for 10 min. Samples were run on NuPage™ Novex™ 4-12% Bis-Tris protein gels in MES buffer or on E-PAGE 8% 48-well gels (ThermoFisher). For native running conditions, NuPAGE Tris-Acetate 3% - 8% gels were used, with buffers as per manufacturer's instructions.

For Western blotting for puromycin and AHA incorporation measurement, chemiluminescence detection was used. Proteins were transferred from the gels to nitrocellulose membranes using an iBlot system (ThermoFisher). Membranes were stained by Ponceau as control for total protein loading, then washed, blocked, and incubated with primary antibody in the blocking buffer at 4°C overnight. Anti-puromycin antibody (PMY-2A4-2 from Developmental Studies Hybridoma bank, at 1:1000) was used with 5% milk in TBST blocking buffer, and an anti-mouse HRP-conjugated secondary antibody, while AHA-biotin was detected using Strep-HRP antibody (R-1098-1 from EpiGentek at 1:2000) in 1% BSA, 0.2% Triton X100 PBS blocking buffer, with additional 10% BSA blocking step before detection. Immobilon reagents (Millipore) were used to detect chemiluminescence. Images were analysed by densitometry in ImageLab v4.1 (BioRad).

For Western blotting of total and p-eIF2a, LICOR protocols and reagents were used. Briefly, methanol-activated PVDF-FL (Immobilon) membranes were utilised for transfer, and dried for 1h before blocking. After re-activation, membranes were blocked in Intercept TBS buffer.

Primary (AHO0802 from ThermoFisher, ab32157 from Abcam, both at 1:1000) and secondary (IRDye 680RD and IRDye 800CW) antibodies were diluted in Intercept TBS buffer with addition of 0.2% Tween-20. Fluorescence was detected and quantified in Odyssey® CLx Imaging system.

Proteasome activity assays

Cell-based ProteasomeGlo™ chymotrypsin-like and trypsin-like assays (Promega) were performed according to manufacturer's instructions (Moravec *et al*, 2009) at multiple circadian timepoints as indicated. Briefly, cells in 96-well plates and the assay reagent were equilibrated to room temperature, before reagent addition, mixing, incubation for 10 min, and luminescence measurement with Tecan Spark 10M plate reader, with integration time of 1 s per well. For analysis, bioluminescence from negative control wells (containing only culture medium and the assay reagent, but no cells) was subtracted from all the experimental conditions.

Aggregation assays

PROTEOSTAT® Aggresome Detection kit (Enzo Life Sciences) was used for detection of protein aggregates (Shen *et al*, 2011). Cells in 96-well plates were treated with MG132 (as indicated in the figure legends), added as 10x bolus diluted in serum-free DMEM to the pre-existing culture media, and gently titurated, to avoid cellular rhythms resetting. Cells were permeabilised and stained simultaneously with PROTEOSTAT® dye and Hoechst 33342, as per kit manufacturer's manual. Total fluorescence in blue and red channels, and representative images of individual wells were acquired using Tecan Spark Cyto plate reader.

Viability assays

PrestoBlue™ High Sensitivity reagent (ThermoFisher), a resazurin-based dye, was used to measure cellular viability (Boncler *et al*, 2014; Xu *et al*, 2015). Cells in 96-well plates were treated with drugs or DMSO (vehicle) controls, as indicated in figure legends, added as 10x bolus diluted in serum-free DMEM on top of existing culture media. For drug washout in the timecourse experiments, cell medium was replaced with 1% serum DMEM, to allow recovery for 18 h. The assay was then performed in line with manufacturer's guidelines: following

PrestoBlue reagent addition and incubation at 37°C for 20 min, fluorescence was measured in a Tecan Spark 10M plate reader, with excitation at 550 nm and emission at 600 nm.

General statistics

Statistical tests were performed using GraphPad Prism (v8 and v9) and R v4, and are indicated in figure legends. *P* values are either reported in figures directly, or annotated with asterisks: * $p \leq 0.05$; ** $p \leq 0.01$, *** $p \leq 0.001$; **** $p \leq 0.0001$, *ns* not significant, $p>0.05$. Number of replicates are reported as *n* or *N* (for technical and biological, respectively) in the figures; error bars represent standard error (SEM) unless stated otherwise. In cases where comparison of fits was performed, determining whether the data are better described by a straight line or a cosine wave with circadian period, the following equation was used for the latter:

$$y = (mx + c) + ae^{kx} \cos \frac{2\pi x - r}{p}$$

Where *m* is the baseline, *c* is the offset from 0 in y-axis, *a* is the amplitude, *k* is the damping rate, *r* is the phase, and *p* is the period.

Proteomics data collection and analysis

Cell culture and sample collection for pSILAC-TMT

For pSILAC-TMT experiments, mouse lung fibroblasts were cultured in 10% dialysed FBS (dFBS). SILAC labelling was conducted in DMEM supplemented with 1% dialysed FBS and heavy-labelled amino acids instead of their light analogues, specifically 84 mg/L $^{13}C_6{}^{15}N_4$ L-Arginine and 146 mg/L $^{13}C_6{}^{15}N_2$ L-Lysine (Ong *et al*, 2002). In the first timecourse pSILAC experiment, sets of cells were labelled for 6h, every 6h over two days, and total cell lysates were extracted in urea/thiourea-based buffer. In the second timecourse experiments, labelling was done for 1.5h, every 6h over two days in duplicates, and fractionation performed as described below. For the booster channel, a fully-heavy labelled sample was used, where cells were cultured in DMEM with heavy amino acids for 5 passages (3-4 w) but otherwise processed in the same way as the timecourse samples. Fractionation was based on LOPIT-DC protocol (Geladaki *et al*, 2019). Two 15cm dishes per sample were used, cells were scraped

in ice-cold PBS, centrifuged, and then lysed on ice by resuspension in a mild buffer (0.25 M sucrose, 10 mM HEPES pH 7.4, 2 mM EDTA, 2 mM magnesium acetate, protease inhibitors) and passaged through a Dounce homogeniser. Lysates were moved to thick-wall ultracentrifuge tubes (Beckman 343778 11mm/34mm) and centrifuged at 79 000 *g* for 43 min to pellet membranes and organelles. Supernatant was then centrifuged again at 120 000 *g* for 45 min. Resulting pellet was resuspended in 8 M urea 20 mM Tris buffer, and processed for mass spectrometry analysis.

Mass spectrometry analysis

Protein digestion

Protein samples were reduced with 5 mM DTT at 56°C for 30 min and alkylated with 10 mM iodoacetamide in the dark at room temperature for 30 min. The samples were then diluted to 3M urea and digested with Lys-C (Promega) for 4 h at 25°C. Next, the samples were further diluted to 1.6 M urea and were digested with trypsin (Promega) overnight, at 30°C. After digestion, an equal volume of ethyl acetate was added and acidified with formic acid (FA) to a final concentration of 0.5%, mixed by shaking for 3 min and centrifuged at 15700 *g* for 2 min. The top organic layer was removed and the bottom aqueous phase was desalted using home-made C18 stage tips (3M Empore) filled with porous R3 resin (Applied Biosystems). The stage tips were equilibrated with 80% acetonitrile (MeCN) and 0.5% FA, followed by 0.5% FA. Bound peptides were eluted with 30-80% MeCN and 0.5% FA and lyophilized.

Tandem mass tag (TMT) labelling

Dried peptide mixtures (50 µg) from each condition were resuspended in 24 µl of 200 mM HEPES, pH 8.5. 12 µl (300 µg) TMTpro 16plex or 18plex reagent (ThermoFisher) reconstituted according to manufacturer's instructions was added and incubated at room temperature for 1 h. The labelling reaction was then terminated by incubation with 2.2 µl 5% hydroxylamine for 30 min. The labelled peptides were pooled into a single sample and desalted using the same stage tips method as above.

Off-line high pH reverse-phase peptides fractionation

200 µg of the labelled peptides were separated on an off-line, high pressure liquid chromatography (HPLC). The experiment was carried out using XBridge BEH130 C18, 5 µm, 2.1 x 150 mm column (Waters), connected to an Ultimate 3000 analytical HPLC (Dionex). Peptides were separated with a gradient of 1-90% buffer A and B (A: 5% MeCN, 10 mM ammonium bicarbonate, pH8; B: MeCN, 10 mM ammonium bicarbonate, pH8, [9:1]) in 60 min at a flow rate of 250 µl/min. A total of 54 fractions were collected, which were then combined into 18 fractions and lyophilized. Dried peptides were resuspended in 1% MeCN and 0.5% FA, and desalted using C18 stage tips, ready for mass spectrometry analysis.

Mass spectra acquisition

The fractionated peptides were analysed by LC-MS/MS using a fully automated Ultimate 3000 RSLC nano System (ThermoFisher) fitted with a 100 µm x 2 cm PepMap100 C18 nano trap column and a 75 µm×25 cm, nanoEase M/Z HSS C18 T3 column (Waters). Peptides were separated by a non-linear gradient of 120 min, 6-38% buffer B (80% MeCN, 0.1% FA). Eluted peptides were introduced directly via a nanoFlex ion source into an Orbitrap Eclipse mass spectrometer (ThermoFisher). Data were acquired using FAIMS-Pro device, running MS3_RTS analysis, switching between two compensation voltages (CV) of -50 and -70 V.

MS1 spectra were acquired using the following settings: R = 120K; mass range = 400-1400 m/z; AGC target = 4e5; MaxIT = 50 ms. Charge states 2-5 were included and dynamic exclusion was set at 60 s. MS2 analysis were carried out with collision induced dissociation (CID) activation, ion trap detection, AGC = 1e4, MaxIT = 35 ms, CE = 34%, and isolation window = 0.7 m/z. RTS-SPS-MS3 was set up to search Uniport *Mus musculus* proteome (2021), with fixed modifications cysteine carbamidomethylation and TMTpro at the peptide N-terminal. TMTpro K, Arg10 (R +10.008), TMTpro K+K8 (K +312.221) and methionine oxidation were set as dynamic modifications. Missed cleavages were allowed, and maximum variable modifications was set at 3. In MS3 scans, the selected precursors were fragmented by high-collision dissociation (HCD), and analysed using the orbitrap with the following settings: isolation window = 0.7 m/z, NCE = 55, orbitrap resolution = 50K, scan range = 110-500 m/z, MaxIT = 200ms, and AGC = 1e5.

Raw MS data processing

The acquired 18 raw files from LC-MS/MS were each split into two individual spectra, one with CV = -50V and one with CV = -70V, total 36 files, using FreeStyle software (ThermoFisher). These files were then processed using MaxQuant (Cox & Mann, 2008) with the integrated Andromeda search engine (v1.6.17.0). MS/MS spectra were quantified with reporter ion MS3 from TMTpro experiments and searched against UniProt *Mus musculus* Reviewed (Nov 2020) Fasta databases. Carbamidomethylation of cysteines was set as a fixed modification, while methionine oxidation, N-terminal acetylation, Arg10 and Lys8 were set as variable modifications.

Data analysis

After the MaxQuant search, all subsequent proteomics data processing and analysis was performed in R (v3.6.1 and v4.1.2) with R Studio v1.2. The custom scripts are available via a github repository, at https://github.com/estere-sei/circadian-pSILAC

Peptide level information from MaxQuant (evidence.txt output file) was used as a starting point. Contaminants and reverse hits were removed. Peptides were classified according to their labelling state: those that had at least one heavy arginine (Arg10) or lysine (Lys8) were classified as “heavy”, and the rest were classified as “light”. Entries for peptides with identical sequences in the same labelling state were grouped together (i.e. their reporter ion intensities across the 16 TMT channels were summed up), including peptides with other modifications such as methionine oxidation. Peptides with missing values were excluded. Total heavy label incorporation was quantified as overall proportion of summed intensities of heavy peptides over total summed intensities per TMT channel. Sample loading normalisation was performed, applying a scaling factor to equalise total summed intensity across TMT channels.

Peptides were filtered to leave only those that were detected in both heavy and light form. Peptide intensities belonging to the same leading razor protein accession were summed up to get total protein abundance value, while the sum of heavy peptides only for each protein

represented the amount of synthesis. The ratio of heavy to total protein intensity averaged across the 8 timepoints was used to estimate relative turnover.

Several methods were used to assess the likelihood of significant circadian change over time in proteins' total abundance and synthesis, including Rhythmicity Analysis Incorporating Non-parametric Methods (RAIN) (Thaben & Westermark, 2014) and ANOVA. With RAIN, the data were tested for rhythms with period length of 24 h. For ANOVA, the data were log-transformed, and two days of sampling were treated as replicates. Oscillation phase was taken from RAIN outputs, and represented circadian time of the peak of oscillation. The extent of change over time is expressed as fold-change, taking average ratio of peak to trough intensity values across the two days of sampling.

For protein complex membership analysis, a list was taken from Ori et al., 2016 which combined CORUM, COMPLEAT and manually annotated complexes and their subunits (Ori *et al*, 2016; Giurgiu *et al*, 2019; Vinayagam *et al*, 2013). Ensembl gene identifiers were converted from human to mouse by g:Profiler g:Orth tool (Raudvere *et al*, 2019), and matched with detected proteins. To asses variability of complex turnover, an analysis similar to one in Mathieson et al., 2018 was performed: standard deviation of the average relative turnover was calculated between proteins belonging to each detected complex, taking only complexes with more than 4 subunits, and compared to a dataset of the same size and structure but with proteins chosen randomly from all detected proteins (i.e. same number of complexes with same number of subunits as in annotated data but "subunits" chosen by random sampling).

For gene ontology functional enrichment analysis, GOrilla tool was used (Eden *et al*, 2009), comparing target protein list with all detected proteins as background, and setting FDR q-value cutoff at 0.05. REVIGO (0.4) was used to remove redundant terms. For analysis of protein-protein interactions, STRING web app was used (Szklarczyk *et al*, 2021), filtering for high-confidence physical interactions, and looking for enrichment against the background of detected proteins.

Mouse tissue experiments

All animal work was licensed by the Home Office under the Animals (Scientific Procedures) Act 1986, with Local Ethical Review by the Medical Research Council and the University of Cambridge, UK. Throughout the experiments, wild-type C57 mice were housed in 12:12 h light:dark conditions.

For *in vivo* turnover measurements, mice received i.p. injections of either 40 µmol/kg puromycin (Ravi *et al*, 2020; Schmidt *et al*, 2009; Ravi *et al*, 2018), or 40 µmol/kg puromycin in combination with 2.5 mg/kg BTZ (Apex Bio). Both solutions were sterile-filtered in PBS with 1% DMSO. Animals were culled 45 min after, in the same order as injected, and livers collected and flash frozen in liquid nitrogen. The procedure was performed twice on the same day, 1 h after the transition from dark to light (ZT1), and 1 h after the transition from light to dark (ZT13). Four age-matched male mice were used per condition.

For *in vivo* response to proteotoxic stress measurements, mice received i.p. injections of 2.5 mg/kg BTZ (Apex Bio) or vehicle control (1% DMSO in PBS, sterile-filtered). Animals were culled 5 h after, in the same order as injected, and livers collected and flash frozen in liquid nitrogen. Injections were performed twice on the same day, 1 h after the transition from dark to light (ZT1), and 1 h after the transition from light to dark (ZT13). 6 age-matched male mice were used per condition.

Tissues were homogenised in urea/thiourea lysis buffers in Precellys 24 Tissue Homogeniser (Bertin Instruments), using CK14 ceramic beads, for 3 x 15 s at 5000 rpm with 30 s breaks. Lysates were then cleared by centrifugation at 14000 rpm for 5 min, followed by protein sample preparation and Western blotting as previously described.

Acknowledgements

We thank all members of O'Neill lab, Rachel Edgar, Manu Hegde and Szymon Juszkiewicz for valuable feedback and discussions, as well as Kathryn Lilley and Holger Kramer for advice on proteomics. We also thank biomedical technical staff at Medical Research Council (MRC) Ares

facility and LMB facilities for assistance. NMR was supported by the Medical Research Council (MR/S022023/1). JON was supported by the Medical Research Council (MC_UP_1201/4).

Author contributions

ES and JON designed the study, analysed the data and wrote the manuscript; SYP-C performed mass spectrometry; NMR, AZ and JON performed mouse studies; ES and AZ performed cell experiments; DCSW and ADB provided further experimental assistance and valuable intellectual contributions. All authors commented on the manuscript.

References

Abramoff MD, Magalhães PJ & Ram SJ (2004) Image processing with ImageJ. *Biophotonics international* 11: 36

Adegoke OAJ, Beatty BE, Kimball SR & Wing SS (2019) Interactions of the super complexes: When mTORC1 meets the proteasome. *International Journal of Biochemistry and Cell Biology* 117

Albornoz N, Bustamante H, Soza A & Burgos P (2019) Cellular Responses to Proteasome Inhibition: Molecular Mechanisms and Beyond. *Int J Mol Sci* 20

Andreani TS, Itoh TQ, Yildirim E, Hwangbo D-S & Allada R (2015) Genetics of Circadian Rhythms. *Sleep Med Clin* 10: 413

Atger F, Gobeta C, Marquis J, Martin E, Wang J, Weger B, Lefebvre G, Descombes P, Naef F & Gachon F (2015) Circadian and feeding rhythms differentially affect rhythmic mRNA transcription and translation in mouse liver. *Proc Natl Acad Sci U S A* 112: E6579–E6588

Atger F, Mauvoisin D, Weger B, Gobet C & Gachon F (2017) Regulation of Mammalian Physiology by Interconnected Circadian and Feeding Rhythms. *Front Endocrinol (Lausanne)* 8

Aviner R (2020) The science of puromycin: From studies of ribosome function to applications in biotechnology. *Comput Struct Biotechnol J* 18: 1074–1083

Bagert JD, Xie YJ, Sweredoski MJ, Qi Y, Hess S, Schuman EM & Tirrell DA (2014) Quantitative, time-resolved proteomic analysis by combining bioorthogonal noncanonical amino acid tagging and pulsed stable isotope labeling by amino acids in cell culture. *Mol Cell Proteomics* 13: 1352–8

Balsalobre A, Damiola F & Schibler U (1998) A serum shock induces circadian gene expression in mammalian tissue culture cells. *Cell* 93: 929–937

Ben-Sahra I & Manning BD (2017) mTORC1 signaling and the metabolic control of cell growth. *Curr Opin Cell Biol* 45: 72–82

Bolitho SJ, Naismith SL, Rajaratnam SMW, Grunstein RR, Hodges JR, Terpening Z, Rogers N & Lewis SJG (2014) Disturbances in melatonin secretion and circadian sleep-wake regulation in Parkinson disease. *Sleep Med* 15: 342–347

Boncler M, Rózalski M, Krajewska U, Podswdek A & Watala C (2014) Comparison of PrestoBlue and MTT assays of cellular viability in the assessment of anti-proliferative effects of plant extracts on human endothelial cells. *J Pharmacol Toxicol Methods* 69: 9–16

Buchan JR & Parker R (2009) Eukaryotic Stress Granules: The Ins and Out of Translation. *Mol Cell* 36: 932

Buhr ED, Yoo SH & Takahashi JS (2010) Temperature as a universal resetting cue for mammalian circadian oscillators. *Science (1979)* 330: 379–385

Buttgereit F & Brand MD (1995) A hierarchy of ATP-consuming processes in mammalian cells. *Biochemical Journal* 312: 163–167

Cao R (2018) mTOR signaling, translational control, and the circadian clock. *Front Genet* 9: 367

Cederroth CR, Albrecht U, Bass J, Brown SA, Dyhrfjeld-Johnsen J, Gachon F, Green CB, Hastings MH, Helfrich-Förster C, Hogenesch JB, *et al* (2019) Medicine in the Fourth Dimension. *Cell Metab* 30: 238–250

Cox J & Mann M (2008) MaxQuant enables high peptide identification rates, individualized p.p.b.-range mass accuracies and proteome-wide protein quantification. *Nat Biotechnol* 26: 1367–72

Cox KH & Takahashi JS (2019) Circadian clock genes and the transcriptional architecture of the clock mechanism. *J Mol Endocrinol* 63: R93–R102

Crosby P, Hamnett R, Putker M, Hoyle NP, Reed M, Karam CJ, Maywood ES, Stangherlin A, Chesham JE, Hayter EA, *et al* (2019) Insulin/IGF-1 Drives PERIOD Synthesis to Entrain Circadian Rhythms with Feeding Time. *Cell* 177: 896-909.e20

Crosby P, Hoyle NP & O'Neill JS (2017) Flexible Measurement of Bioluminescent Reporters Using an Automated Longitudinal Luciferase Imaging Gas- and Temperature-optimized Recorder (ALLIGATOR). *J Vis Exp*

Dantuma NP & Lindsten K (2010) Stressing the ubiquitin-proteasome system. *Cardiovasc Res* 85: 263–271

Delarue M, Brittingham GP, Pfeffer S, Surovtsev I v., Pinglay S, Kennedy KJ, Schaffer M, Gutierrez JI, Sang D, Poterewicz G, *et al* (2018) mTORC1 Controls Phase Separation and the Biophysical Properties of the Cytoplasm by Tuning Crowding. *Cell* 174: 338-349.e20

Deshaies RJ (2014) Proteotoxic crisis, the ubiquitin-proteasome system, and cancer therapy. *BMC Biology 2014 12:1* 12: 1–14

Desvergne A, Ugarte N, Radjei S, Gareil M, Petropoulos I & Friguet B (2016) Circadian modulation of proteasome activity and accumulation of oxidized protein in human embryonic kidney HEK 293 cells and primary dermal fibroblasts. *Free Radic Biol Med* 94: 195–207

Dibner C, Schibler U & Albrecht U (2010) The mammalian circadian timing system: organization and coordination of central and peripheral clocks. *Annu Rev Physiol* 72: 517–549

Dimitrova LN, Kuroha K, Tatematsu T & Inada T (2009) Nascent Peptide-dependent Translation Arrest Leads to Not4p-mediated Protein Degradation by the Proteasome. *J Biol Chem* 284: 10343

Doherty MK, Hammond DE, Clague MJ, Gaskell SJ & Beynon RJ (2009) Turnover of the Human Proteome: Determination of Protein Intracellular Stability by Dynamic SILAC. *J Proteome Res* 8: 104–112

Eden E, Navon R, Steinfeld I, Lipson D & Yakhini Z (2009) GOrilla: A tool for discovery and visualization of enriched GO terms in ranked gene lists. *BMC Bioinformatics* 10: 1–7

Feeney KA, Hansen LL, Putker M, Olivares-Yañez C, Day J, Eades LJ, Larrondo LF, Hoyle NP, O'Neill JS & van Ooijen G (2016a) Daily magnesium fluxes regulate cellular timekeeping and energy balance. *Nature* 532: 375–9

Feeney KA, Putker M, Brancaccio M & O'Neill JS (2016b) In-depth Characterization of Firefly Luciferase as a Reporter of Circadian Gene Expression in Mammalian Cells. *J Biol Rhythms* 31: 540

Gandin V & Topisirovic I (2014) Co-translational mechanisms of quality control of newly synthesized polypeptides. *Translation* 2: e28109

Geladaki A, Kočevar Britovšek N, Breckels LM, Smith TS, Vennard OL, Mulvey CM, Crook OM, Gatto L & Lilley KS (2019) Combining LOPIT with differential ultracentrifugation for high-resolution spatial proteomics. *Nature Communications 2019 10:1* 10: 1–15

Giurgiu M, Reinhard J, Brauner B, Dunger-Kaltenbach I, Fobo G, Frishman G, Montrone C & Ruepp A (2019) CORUM: The comprehensive resource of mammalian protein complexes - 2019. *Nucleic Acids Res* 47: D559–D563

Goodman CA & Hornberger TA (2013) Measuring protein synthesis with SUnSET: A valid alternative to traditional techniques? *Exerc Sport Sci Rev* 41: 107–115

Harper JW & Bennett EJ (2016) Proteome complexity and the forces that drive proteome imbalance. *Nature* 537: 328–338

Hipp MS, Kasturi P & Hartl FU (2019) The proteostasis network and its decline in ageing. *Nature Reviews Molecular Cell Biology 2019 20:7* 20: 421–435

Hoyle NP, Seinkmane E, Putker M, Feeney KA, Krogager TP, Chesham JE, Bray LK, Thomas JM, Dunn K, Blaikley J, *et al* (2017) Circadian actin dynamics drive rhythmic fibroblast mobilization during wound healing. *Sci Transl Med* 9: eaal2774

Hughes ME, Abruzzi KC, Allada R, Anafi R, Arpat AB, Asher G, Baldi P, de Bekker C, Bell-Pedersen D, Blau J, *et al* (2017) Guidelines for Genome-Scale Analysis of Biological Rhythms. *J Biol Rhythms* 32: 380–393

Jang C, Lahens NF, Hogenesch JB & Sehgal A (2015a) Ribosome profiling reveals an important role for translational control in circadian gene expression. *Genome Res* 25: 1836–47

Jang C, Lahens NF, Hogenesch JB & Sehgal A (2015b) Ribosome profiling reveals an important role for translational control in circadian gene expression. *Genome Res* 25: 1836–47

Janich P, Arpat AB, Castelo-Szekely V, Lopes M & Gatfield D (2015) Ribosome profiling reveals the rhythmic liver translatome and circadian clock regulation by upstream open reading frames. *Genome Res* 25: 1848–59

Jiang H-Y & Wek RC (2005) Phosphorylation of the alpha-subunit of the eukaryotic initiation factor-2 (eIF2alpha) reduces protein synthesis and enhances apoptosis in response to proteasome inhibition. *J Biol Chem* 280: 14189–202

Jouffe C, Cretenet G, Symul L, Martin E, Atger F, Naef F & Gachon F (2013) The Circadian Clock Coordinates Ribosome Biogenesis. *PLoS Biol* 11: e1001455

Juszkiewicz S & Hegde RS (2018) Quality Control of Orphaned Proteins. *Mol Cell* 71: 443–457

Karki S, Castillo K, Ding Z, Kerr O, Lamb TM, Wu C, Sachs MS & Bell-Pedersen D (2020) Circadian clock control of eIF2α phosphorylation is necessary for rhythmic translation initiation. *Proc Natl Acad Sci U S A* 117: 10935–10945

Kay H, Grünewald E, Feord HK, Gil S, Peak-Chew SY, Stangherlin A, O'Neill JS & van Ooijen G (2021) Deep-coverage spatiotemporal proteome of the picoeukaryote Ostreococcus tauri reveals differential effects of environmental and endogenous 24-hour rhythms. *Commun Biol* 4: 1147

Kelu JJ, Pipalia TG & Hughes SM (2020) Circadian regulation of muscle growth independent of locomotor activity. *Proceedings of the National Academy of Sciences* 117: 31208–31218

Labbadia J & Morimoto RI (2015) The biology of proteostasis in aging and disease. *Annu Rev Biochem* 84: 435–464

Lane N & Martin W (2010) The energetics of genome complexity. *Nature* 467: 929–934

Leng Y, Musiek ES, Hu K, Cappuccio FP & Yaffe K (2019) Association between circadian rhythms and neurodegenerative diseases. *Lancet Neurol* 18: 307

Lipton JO, Boyle LM, Yuan ED, Hochstrasser KJ, Chifamba FF, Nathan A, Tsai PT, Davis F & Sahin M (2017) Aberrant Proteostasis of BMAL1 Underlies Circadian Abnormalities in a Paradigmatic mTOR-opathy. *Cell Rep* 20: 868

Lipton JO, Yuan ED, Boyle LM, Ebrahimi-Fakhari D, Kwiatkowski E, Nathan A, Güttler T, Davis F, Asara JM & Sahin M (2015) The Circadian Protein BMAL1 Regulates Translation in Response to S6K1-Mediated Phosphorylation. *Cell* 161: 1138–1151

Liu TY, Huang HH, Wheeler D, Xu Y, Wells JA, Song YS & Wiita AP (2017) Time-Resolved Proteomics Extends Ribosome Profiling-Based Measurements of Protein Synthesis Dynamics. *Cell Syst* 4: 636-644.e9

Malcolm M, Saad L, Penazzi LG & Garbarino-Pico E (2019) Processing Bodies Oscillate in Neuro 2A Cells. *Front Cell Neurosci* 13: 487

Manasanch EE & Orlowski RZ (2017) Proteasome inhibitors in cancer therapy. *Nat Rev Clin Oncol* 14: 417–433

Mathieson T, Franken H, Kosinski J, Kurzawa N, Zinn N, Sweetman G, Poeckel D, Ratnu VS, Schramm M, Becher I, *et al* (2018) Systematic analysis of protein turnover in primary cells. *Nat Commun* 9: 689

Mauvoisin D & Gachon F (2019) Proteomics in Circadian Biology. *J Mol Biol*

Mauvoisin D, Wang J, Jouffe C, Martin E, Atger F, Waridel P, Quadroni M, Gachon F & Naef F (2014) Circadian clock-dependent and -independent rhythmic proteomes implement distinct diurnal functions in mouse liver. *Proc Natl Acad Sci U S A* 111: 167–72

Mei W, Jiang Z, Chen Y, Chen L, Sancar A & Jiang Y (2021) Genome-wide circadian rhythm detection methods: systematic evaluations and practical guidelines. *Brief Bioinform* 22: 1–13

Moravec RA, O'Brien MA, Daily WJ, Scurria MA, Bernad L & Riss TL (2009) Cell-based bioluminescent assays for all three proteasome activities in a homogeneous format. *Anal Biochem* 387: 294–302

Musiek ES, Bhimasani M, Zangrilli MA, Morris JC, Holtzman DM & Ju YES (2018) Circadian rest-activity pattern changes in aging and preclinical Alzheimer disease. *JAMA Neurol* 75: 582–590

Nathans D (1964) PUROMYCIN INHIBITION OF PROTEIN SYNTHESIS: INCORPORATION OF PUROMYCIN. *Proceedings of the National Academy of Sciences of the United States of* 51: 585–592

O'Neill JS, Hoyle NP, Robertson JB, Edgar RS, Beale AD, Peak-Chew SY, Day J, Costa ASH, Frezza C & Causton HC (2020) Eukaryotic cell biology is temporally coordinated to support the energetic demands of protein homeostasis. *Nat Commun* 11

Ong S-E, Blagoev B, Kratchmarova I, Kristensen DB, Steen H, Pandey A & Mann M (2002) Stable isotope labeling by amino acids in cell culture, SILAC, as a simple and accurate approach to expression proteomics. *Mol Cell Proteomics* 1: 376–86

Ori A, Iskar M, Buczak K, Kastritis P, Parca L, Andrés-Pons A, Singer S, Bork P & Beck M (2016) Spatiotemporal variation of mammalian protein complex stoichiometries. *Genome Biol* 17: 1–15

Pathak SS, Liu D, Li T, de Zavalia N, Zhu L, Li J, Karthikeyan R, Alain T, Liu AC, Storch KF, *et al* (2019) The eIF2α Kinase GCN2 Modulates Period and Rhythmicity of the Circadian Clock by Translational Control of Atf4. *Neuron* 104: 724-735.e6

Price JC, Guan S, Burlingame A, Prusiner SB & Ghaemmaghami S (2010) Analysis of proteome dynamics in the mouse brain. *Proc Natl Acad Sci U S A* 107: 14508–14513

Ramanathan C, Kathale ND, Liu D, Lee C, Freeman DA, Hogenesch JB, Cao R & Liu AC (2018) mTOR signaling regulates central and peripheral circadian clock function. *PLoS Genet* 14: e1007369

Raudvere U, Kolberg L, Kuzmin I, Arak T, Adler P, Peterson H & Vilo J (2019) g:Profiler: a web server for functional enrichment analysis and conversions of gene lists (2019 update). *Nucleic Acids Res* 47: W191–W198

Ravi V, Jain A, Ahamed F, Fathma N, Desingu PA & Sundaresan NR (2018) Systematic evaluation of the adaptability of the non-radioactive SUnSET assay to measure cardiac protein synthesis. *Scientific Reports 2018 8:1* 8: 1–11

Ravi V, Jain A, Mishra S & Sundaresan NR (2020) Measuring Protein Synthesis in Cultured Cells and Mouse Tissues Using the Non-radioactive SUnSET Assay. *Curr Protoc Mol Biol* 133: e127

Reddy AB, Karp NA, Maywood ES, Sage EA, Deery M, O'Neill JS, Wong GKY, Chesham J, Odell M, Lilley KS, *et al* (2006) Circadian orchestration of the hepatic proteome. *Curr Biol* 16: 1107–15

Ribatti D (2017) A revisited concept: Contact inhibition of growth. From cell biology to malignancy. *Exp Cell Res* 359: 17–19 doi:10.1016/j.yexcr.2017.06.012 [PREPRINT]

Riggs CL, Kedersha N, Ivanov P & Anderson P (2020) Mammalian stress granules and P bodies at a glance. *J Cell Sci* 133

Robles MS, Cox J & Mann M (2014) In-Vivo Quantitative Proteomics Reveals a Key Contribution of Post-Transcriptional Mechanisms to the Circadian Regulation of Liver Metabolism. *PLoS Genet* 10: e1004047

Ross AB, Langer JD & Jovanovic M (2021) Proteome turnover in the spotlight: Approaches, applications, and perspectives. *Molecular and Cellular Proteomics* 20

Ryzhikov M, Ehlers A, Steinberg D, Xie W, Oberlander E, Brown S, Gilmore PE, Townsend RR, Lane WS, Dolinay T, *et al* (2019) Diurnal Rhythms Spatially and Temporally Organize Autophagy. *Cell Rep* 26: 1880-1892.e6

Santiago AM, Gonçalves DL & Morano KA (2020) Mechanisms of sensing and response to proteotoxic stress. *Exp Cell Res* 395: 112240

Schindelin J, Arganda-Carreras I, Frise E, Kaynig V, Longair M, Pietzsch T, Preibisch S, Rueden C, Saalfeld S, Schmid B, *et al* (2012) Fiji: an open-source platform for biological-image analysis. *Nature Methods 2012 9:7* 9: 676–682

Schmidt EK, Clavarino G, Ceppi M & Pierre P (2009) SUnSET, a nonradioactive method to monitor protein synthesis. *Nat Methods* 6: 275–277

Schubert U, Antón LC, Gibbs J, Norbury CC, Yewdell JW & Bennink JR (2000) Rapid degradation of a large fraction of newly synthesized proteins by proteasomes. *Nature* 404: 770–774

Schwanhäusser B, Busse D, Li N, Dittmar G, Schuchhardt J, Wolf J, Chen W & Selbach M (2011) Global quantification of mammalian gene expression control. *Nature* 473: 337–342

Seluanov A, Vaidya A & Gorbunova V (2010) Establishing primary adult fibroblast cultures from rodents. *J Vis Exp*

Semenkov Y, Shapkina T, Makhno V & Kirillov S (1992) Puromycin reaction for the A site-bound peptidyl-tRNA. *FEBS Lett* 296: 207–210

Shen D, Coleman J, Chan E, Nicholson TP, Dai L, Sheppard PW & Patton WF (2011) Novel cell- and tissue-based assays for detecting misfolded and aggregated protein accumulation within aggresomes and inclusion bodies. *Cell Biochem Biophys* 60: 173–85

Sinturel F, Gerber A, Mauvoisin D, Wang J, Gatfield D, Stubblefield JJ, Green CB, Gachon F & Schibler U (2017) Diurnal Oscillations in Liver Mass and Cell Size Accompany Ribosome Assembly Cycles. *Cell* 169: 651-663.e14

Smith PK, Krohn RI, Hermanson GT, Mallia AK, Gartner FH, Provenzano MD, Fujimoto EK, Goeke NM, Olson BJ & Klenk DC (1985) Measurement of protein using bicinchoninic acid. *Anal Biochem* 150: 76–85

Stangherlin A, Seinkmane E & O'Neill JS (2021a) Understanding circadian regulation of mammalian cell function, protein homeostasis, and metabolism. *Curr Opin Syst Biol*: 100391

Stangherlin A, Watson JL, Wong DCS, Barbiero S, Zeng A, Seinkmane E, Chew SP, Beale AD, Hayter EA, Guna A, *et al* (2021b) Compensatory ion transport buffers daily protein rhythms to regulate osmotic balance and cellular physiology. *Nature Communications 2021 12:1* 12: 1–14

Szklarczyk D, Gable AL, Nastou KC, Lyon D, Kirsch R, Pyysalo S, Doncheva NT, Legeay M, Fang T, Bork P, *et al* (2021) The STRING database in 2021: customizable protein-protein networks, and functional characterization of user-uploaded gene/measurement sets. *Nucleic Acids Res* 49: D605–D612

Taggart JC, Zauber H, Selbach M, Li G-W & McShane E (2020) Keeping the Proportions of Protein Complex Components in Check. *Cell Syst* 10: 125–132

Thaben PF & Westermark PO (2014) Detecting rhythms in time series with rain. *J Biol Rhythms* 29: 391–400

Vinayagam A, Hu Y, Kulkarni M, Roesel C, Sopko R, Mohr SE & Perrimon N (2013) Protein Complex–Based Analysis Framework for High-Throughput Data Sets. *Sci Signal* 6: rs5

Wagner PM, Prucca CG, Velazquez FN, Sosa Alderete LG, Caputto BL & Guido ME (2021) Temporal regulation of tumor growth in nocturnal mammals: In vivo studies and chemotherapeutical potential. *The FASEB Journal* 35: e21231

Wang F, Durfee LA & Huibregtse JM (2013) A Cotranslational Ubiquitination Pathway for Quality Control of Misfolded Proteins. *Mol Cell* 50: 368–378

Wang R, Jiang X, Bao P, Qin M & Xu J (2019) Circadian control of stress granules by oscillating EIF2α. *Cell Death Dis* 10: 1–12

Welsh DK, Yoo SH, Liu AC, Takahashi JS & Kay SA (2004) Bioluminescence imaging of individual fibroblasts reveals persistent, independently phased circadian rhythms of clock gene expression. *Current Biology* 14: 2289–2295

Wheatley DN, Giddings MR & Inglis MS (1980) Kinetics of degradation of 'short-' and 'long-lived' proteins in cultured mammalian cells. *Cell Biol Int Rep* 4: 1081–1090

Wolff S, Weissman JS & Dillin A (2014) Differential scales of protein quality control. *Cell* 157: 52–64

Wong DCS, Seinkmane E, Zeng A, Stangherlin A, Rzechorzek NM, Beale AD, Day J, Reed M, Peak-Chew SY, Styles CT, *et al* (2022) CRYPTOCHROMES promote daily protein homeostasis. *EMBO J* 41: e108883

Xu M, McCanna DJ & Sivak JG (2015) Use of the viability reagent PrestoBlue in comparison with alamarBlue and MTT to assess the viability of human corneal epithelial cells. *J Pharmacol Toxicol Methods* 71: 1–7

Yoo S-H, Yamazaki S, Lowrey PL, Shimomura K, Ko CH, Buhr ED, Siepka SM, Hong H-K, Oh WJ, Yoo OJ, *et al* (2004) PERIOD2::LUCIFERASE real-time reporting of circadian dynamics reveals persistent circadian oscillations in mouse peripheral tissues. *Proc Natl Acad Sci U S A* 101: 5339–46

Zhang R, Lahens NF, Ballance HI, Hughes ME & Hogenesch JB (2014) A circadian gene expression atlas in mammals: Implications for biology and medicine. *Proc Natl Acad Sci U S A* 111: 16219–16224

Zhang X, Linder S & Bazzaro M (2020) Drug Development Targeting the Ubiquitin–Proteasome System (UPS) for the Treatment of Human Cancers. *Cancers 2020, Vol 12, Page 902* 12: 902

Figure legends

Figure 1.

a. A representative phosphor screen exposure of SDS-PAGE gel showing ^{35}S-Met/Cys incorporation in 15 min pulse (P) and 1 h chase (C) samples at different circadian times in mouse lung fibroblasts.
b. Quantification of radiolabel signal in pulse and chase at the different timepoints, normalised to protein content (by Coomassie stain). Statistics: two-way ANOVA with Dunnett's multiple comparison test, comparing T24 to other timepoints. On the right, the inferred degradation within 1h of chase is plotted, calculated as 100%*(1-Chase/Pulse). Statistics: one-way ANOVA with Dunnett's multiple comparison test, comparing T24 to other timepoints.
c. Chymotrypsin-like, trypsin-like, and caspase-like proteasome activities, measured by ProteasomeGlo cell-based assays, at different circadian times as indicated. Statistics: damped cosine wave fit compared with straight line (null hypothesis) by extra sum-of-squares F test, the statistically preferred fit is plotted and p-value displayed. Parallel PER2::LUC bioluminescence recording from a replicate cell culture is shown below, acting as phase marker.

d. Schematic representation of the optimised puromycin incorporation assay. Puromycin (Puro) is incorporated into nascent peptide chains during translation elongation, and at least a subset of these gets degraded by the proteasome within a short timeframe; in the presence of bortezomib (BTZ), proteasome is inhibited, so the peptides that would have been degraded are still present and can be detected. Thus, a comparison of the two conditions allows estimation of both translation and degradation.
e. Quantification of total protein, protein synthesis and protein turnover from a puromycin incorporation timecourse, where at each timepoint Puro with or without BTZ was added directly to cell media, and cells lysed 30 min afterwards. Puromycin incorporation was assessed by Western blotting, and total protein from a parallel Ponceau Red stain. Change in degradation was calculated from fitted data of puromycin incorporation, relative to mean degradation level. Statistics: damped cosine wave fit compared with straight line (null hypothesis) by extra sum-of-squares F test, the statistically preferred fit is plotted and p-value displayed. Parallel PER2::LUC bioluminescence recording from a replicate cell culture is shown below, acting as phase marker.
f. Puromycin incorporation *in vivo*: mice received an i.p. injection of puromycin with or without BTZ at ZT1 or ZT13, and livers were harvested 40 min afterwards. Representative anti-puromycin Western blot is shown, and quantification is shown on the right, normalised for protein loading as assessed by Coomassie staining. Statistics: two-way ANOVA with Sidak's multiple comparisons test.

Figure 2.

a. Schematic of circadian pulsed SILAC-TMT experiment design. In a set of entrained fibroblasts, at each circadian timepoint "light" media (DMEM with standard L-Arg and L-Lys) is switched for "heavy" (DMEM with $^{13}C_6{}^{15}N_4$ L-Arg and $^{13}C_6{}^{15}N_2$ L-Lys), and cells lysed after 6h. Lysates are then digested, labelled with tandem mass tags (TMT), mixed and analysed by mass spectrometry.
b. Parallel bioluminescence recording of PER2::LUC, acting as phase marker, overlayed with SILAC labelling windows that were used for the timecourse.
c. Representative examples of proteins changing rhythmically or staying constant in their total abundance (left) or synthesis (right), as measured in the pSILAC-TMT timecourse. Atp6v1c1, V-type proton ATPase subunit C 1, RAIN p=0.03; Cpt1c, Carnitine O-palmitoyltransferase 1, RAIN p=1; Cadm4, Cell adhesion molecule 4, RAIN p=0.0076; Erp29, Endoplasmic reticulum resident protein 29, p=0.92; Nup107, Nuclear pore complex protein Nup107, RAIN p=0.00152; Hspa14, Heat shock 70 kDa protein 14, RAIN p=0.00762
d. Probability density distribution of fold-change between peak and trough for proteins rhythmic in synthesis and in total abundance. Statistics: Mann-Whitney test.
e. Comparison of rhythmicity between individual proteins' synthesis and total abundance. Statistically, significant change over time was assessed by two algorithms, RAIN and ANOVA, with $p<0.05$ taken as rhythmicity threshold. Percentages of detected proteins falling under the four rhythmicity categories by the two algorithms are displayed. Degradation rhythms can account for cases of proteins with rhythms in synthesis but not abundance, or *vice versa*.

f. Phase distribution of proteins rhythmic (with threshold RAIN $p<0.05$) in both synthesis and total abundance, as well as their circadian phase difference. Gene ontology functional enrichment was tested for by GOrilla tool, in each phase separately or together, against the background of all detected proteins, and no terms were significant below the corrected p-value (FDR q-value) 0.05 cutoff.
g. Phase distribution of proteins rhythmic (with threshold RAIN $p<0.05$) in their total abundance and in their synthesis.

Figure 3.

a. Schematic of circadian pulsed SILAC-TMT with extra fractionation step. In a set of entrained fibroblasts, at each circadian timepoint "light" media (DMEM with standard L-Arg and L-Lys) is switched for "heavy" (DMEM with $^{13}C_6{}^{15}N_4$ L-Arg and $^{13}C_6{}^{15}N_2$ L-Lys), and cells collected after 1.5h. Samples were then subjected to sequential ultracentrifugation, a method adjusted from Geladaki et al 2019 LOPIT-DC protocol. The fraction enriched for macromolecular protein complexes (MMC fraction) was labelled with tandem mass tags (TMT), mixed and analysed by mass spectrometry.
b. Parallel bioluminescence recording of PER2::LUC, acting as phase marker, overlayed with SILAC labelling windows that were used for the timecourse.
c. Comparison of percentage of detected proteins that are considered rhythmic ($p<0.05$) in their synthesis by the two algorithms used, between the whole-cell pSILAC experiment, presented in Fig. 2, and the experiment focused on complexes, presented in this figure.
d. Probability density distribution of fold-change between peak and trough for proteins rhythmic in synthesis and in total abundance. Statistics: Mann-Whitney test.
e. Comparison of rhythmicity between individual proteins' synthesis and total abundance. Statistically, significant change over time was assessed by two algorithms, RAIN and ANOVA, with $p<0.05$ taken as rhythmicity threshold. Percentages of detected proteins falling under the four rhythmicity categories by the two algorithms are displayed.
f. Coordinated turnover of proteins belonging to complexes: for four selected complexes, their annotated subunits (according to a compilation of CORUM, COMPLEAT and manual annotations) were averaged in terms of their fold-change over time (x-axis), and relative turnover (proportion of heavy to total peptide intensity averaged across 8 timepoints, y axis). All proteins are displayed in the background in grey. Normalised heavy abundance, i.e. synthesis, of these proteins over time is shown on heatmaps on the right.
g. Proteins rhythmic (RAIN $p<0.05$) in their synthesis were analysed using STRING interaction database, filtering for high-confidence, physical interactions. Proteins with rhythmic synthesis in the complex fraction had an interconnected protein-protein interaction network, with high average node degree and significant enrichment in interactions over all detected proteins in that experiment, whereas for proteins with rhythmic synthesis in the whole-cell experiment (Fig. 2) this was not the case.
h. Fibroblasts were pulsed with AHA for 1.5h at the indicated timepoints, and AHA incorporation into protein complexes and other higher molecular weight species under native conditions, using biotin as click substrate and streptavidin-HRP for

detection after non-denaturing gel electrophoresis. Signal was quantified and normalised to total protein content as measured by SyproRuby, plotted on the right. Statistics: damped cosine wave fit (plotted) preferred over straight line, extra sum-of-squares F test p-value displayed.

Figure 4.

a. Phase distribution of proteins rhythmic (RAIN $p<0.05$) in their total abundance and in their synthesis in the MMC fraction. Gene ontology functional enrichment for biological processes was performed using GOrilla tool, with proteins at each phase compared against all detected proteins in this experiment, and FDR q-value (multiple comparisons adjusted p-value) threshold of 0.05. For phase "24", top significant non-overlapping terms are presented, alongside their significance and fold-enrichment values. In phase "18", terms associated with actin were enriched ($q<0.05$), e.g. "actin filament bundle assembly" (8.85-fold enrichment).
b. Example proteins peaking at phase "24", belonging to terms associated with ribonucleoprotein complex assembly and stress granule assembly. Plotted are their abundance and synthesis in the MMC fraction as well as at whole-cell level (measured independently).
c. Example proteins peaking at phase "18", associated with actin assembly. Plotted are their abundance and synthesis in the MMC fraction as well as at whole-cell level.

Figure 5.

a. Parallel PER2::LUC bioluminescence recording, conducted under the same experimental and timecourse conditions as experiments in b, c & d.
b. Two sets of fibroblast lysates were collected every 4 h for 3 days, one untreated control and one treated with 20 µM MG132 proteasomal inhibitor for 4 h before each collection. Fold-change increase in relative phosphorylation of eIF2α (i.e. $(\text{p-eIF2}\alpha/\text{total})_{MG132}/(\text{p-eIF2}\alpha/\text{total})_{control}$) at each timepoint is plotted. MG132 is expected to induce increase in phosphorylation of eIF2α but the extent of the induction differs. Statistics: damped cosine wave fit (plotted) preferred over straight line, extra sum-of-squares F test p-value displayed.
c. Cells were treated with 20 µM MG132 for 24h starting at indicated timepoints, and aggregation relative to untreated samples measured by Proteastat aggresome kit. MG132 is expected to induce aggregation but the extent of the induction differs. Statistics: One-way ANOVA $p<0.0001$, stars and colours represent Dunnett's multiple comparison of neighbouring timepoints.
d. At 8 timepoints throughout 2 days, fibroblasts were treated with 2.5 µM proteasomal inhibitor bortezomib (BTZ), 25 µM translation inhibitor cycloheximide (CHX), or vehicle control; after 6 h, the drugs were washed out, allowing cells to recover for further 18 h. Cellular viability after the treatments, as measured by PrestoBlue High Sensitivity assay, is expressed as a proportion of control (vehicle-treated) cells at each timepoint. Statistics: damped cosine wave fit compared with straight line (null

hypothesis) by extra sum-of-squares F test, the statistically preferred fit is plotted & p-value displayed.

e. Time-of-day bortezomib (BTZ) effect *in vivo*: mice received an i.p. injection of BTZ or vehicle control (VEH) at ZT1 or ZT13, and livers were harvested 5h after the treatment. Representative Western blot is shown, blots, probed for total (green) and S51-phopshorylated (red) eIF2α.
f. Quantification of relative phosphorylation levels of eIF2α from experiment in e. Statistics: repeated measures two-way ANOVA with Sidak's multiple comparisons test
g. Fold-change increase in phosphorylation of eIF2α upon bortezomib injection, quantified from f. Statistics: paired t-test.

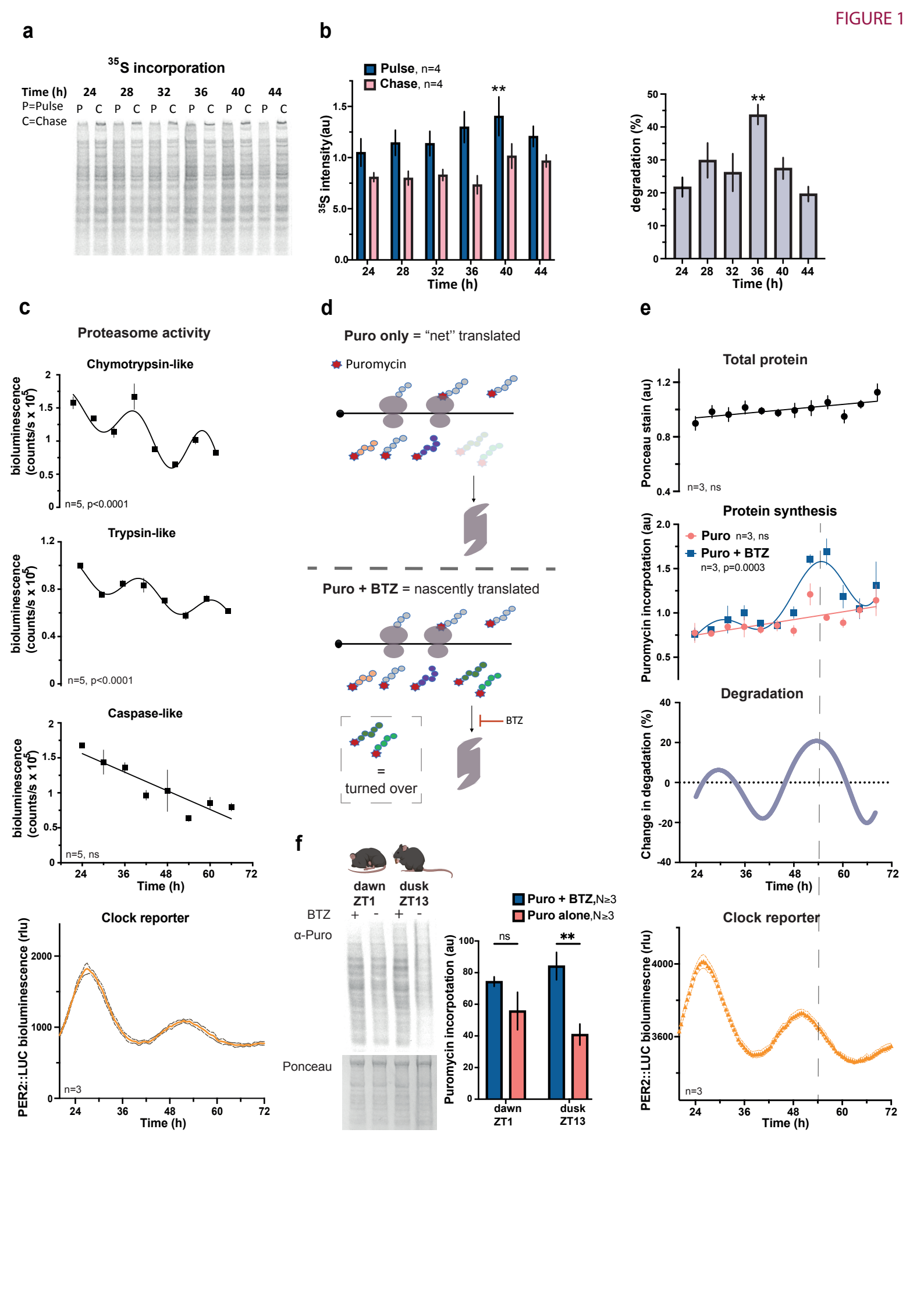
a
35S incorporation
Time (h) 24 28 32 36 40 44
P=Pulse
C=Chase
P C P C P C P C P C P C
b
Pulse, n=4
Chase, n=4
35S intensity(au)
Time (h)
degradation (%)
Time (h)
c
Proteasome activity
Chymotrypsin-like
bioluminescence (counts/s x 10^5)
n=5, p<0.0001
Trypsin-like
n=5, p<0.0001
Caspase-like
n=5, ns
Time (h)
Clock reporter
PER2::LUC bioluminescence (rlu)
n=3
Time (h)
d
Puro only = "net" translated
Puromycin
Puro + BTZ = nascently translated
BTZ
=
turned over
e
Total protein
Ponceau stain (au)
n=3, ns
Protein synthesis
Puromycin incorporation (au)
Puro n=3, ns
Puro + BTZ
n=3, p=0.0003
Degradation
Change in degadation (%)
Time (h)
Clock reporter
PER2::LUC bioluminescne (rlu)
n=3
Time (h)
f
dawn ZT1
dusk ZT13
BTZ + - + -
α-Puro
Ponceau
Puro + BTZ,N≥3
Puro alone,N≥3
ns
Puromycin incorporation (au)
dawn ZT1
dusk ZT13

FIGURE 2

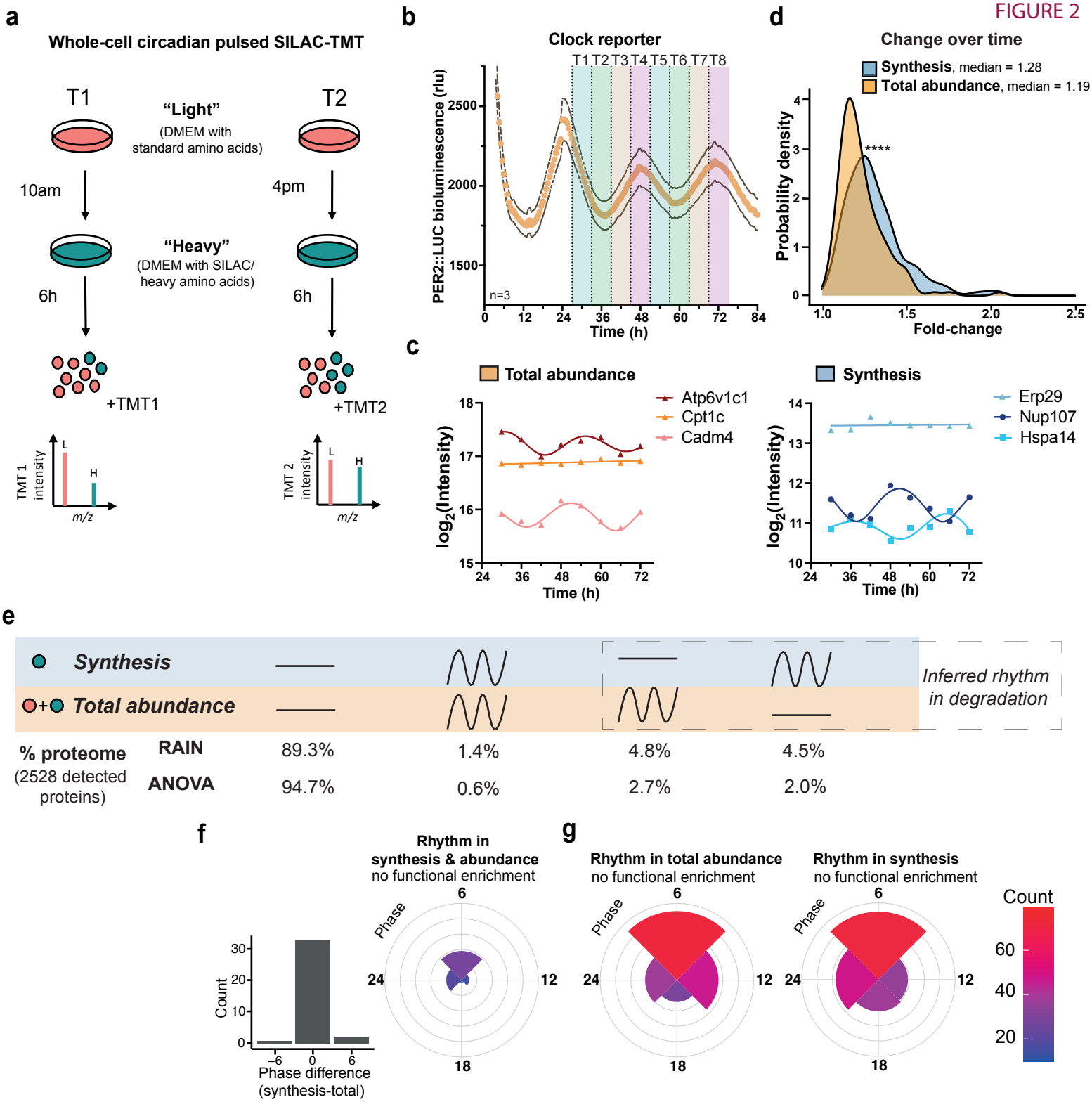
a
Whole-cell circadian pulsed SILAC-TMT
T1
T2
"Light"
(DMEM with standard amino acids)
10am
4pm
"Heavy"
(DMEM with SILAC/ heavy amino acids)
6h
6h
+TMT1
+TMT2
TMT 1 intensity
TMT 2 intensity
L
H
m/z
b
Clock reporter
T1 T2 T3 T4 T5 T6 T7 T8
PER2::LUC bioluminescence (rlu)
n=3
Time (h)
d
Change over time
Synthesis, median = 1.28
Total abundance, median = 1.19
Probability density
****
Fold-change
c
Total abundance
Synthesis
Atp6v1c1
Cpt1c
Cadm4
Erp29
Nup107
Hspa14
log2(Intensity)
Time (h)
e
Synthesis
Total abundance
Inferred rhythm in degradation
% proteome (2528 detected proteins)
RAIN 89.3% 1.4% 4.8% 4.5%
ANOVA 94.7% 0.6% 2.7% 2.0%
f
Count
Phase difference (synthesis-total)
Rhythm in synthesis & abundance
no functional enrichment
Phase
g
Rhythm in total abundance
no functional enrichment
Rhythm in synthesis
no functional enrichment
Count

FIGURE 3

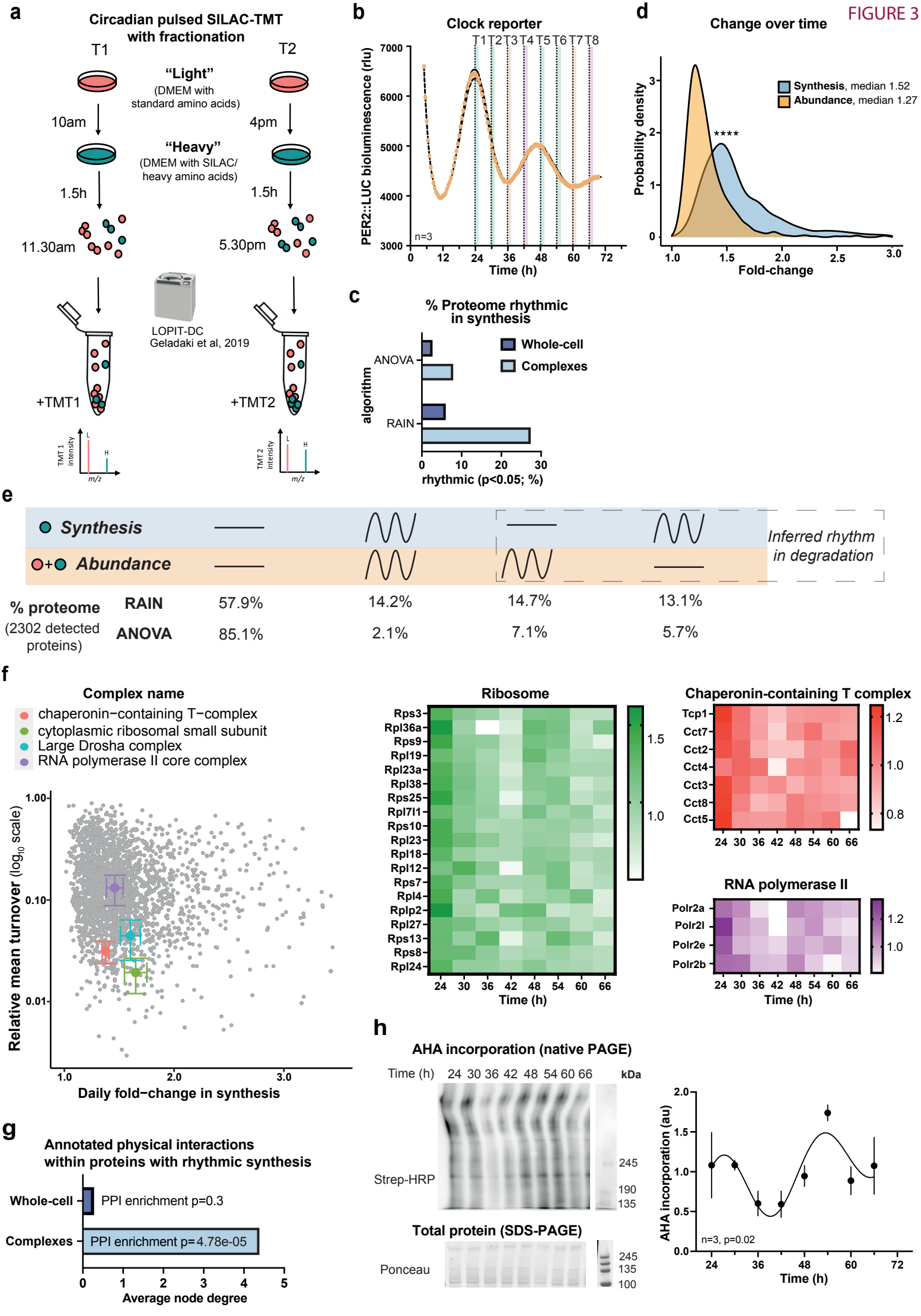
a
Circadian pulsed SILAC-TMT with fractionation
T1
T2
"Light"
(DMEM with standard amino acids)
10am
4pm
"Heavy"
(DMEM with SILAC/ heavy amino acids)
1.5h
1.5h
11.30am
5.30pm
LOPIT-DC
Geladaki et al, 2019
+TMT1
+TMT2
TMT 1 intensity
TMT 2 intensity
m/z
b
Clock reporter
T1 T2 T3 T4 T5 T6 T7 T8
PER2::LUC bioluminescence (rlu)
n=3
Time (h)
c
% Proteome rhythmic in synthesis
Whole-cell
Complexes
ANOVA
RAIN
algorithm
rhythmic (p<0.05; %)
d
Change over time
Synthesis, median 1.52
Abundance, median 1.27
****
Probability density
Fold-change
e
Synthesis
Abundance
Inferred rhythm in degradation
% proteome (2302 detected proteins)
RAIN 57.9% 14.2% 14.7% 13.1%
ANOVA 85.1% 2.1% 7.1% 5.7%
f
Complex name
chaperonin−containing T−complex
cytoplasmic ribosomal small subunit
Large Drosha complex
RNA polymerase II core complex
Relative mean turnover (log10 scale)
Daily fold−change in synthesis
Ribosome
Rps3
Rpl36a
Rps9
Rpl19
Rpl23a
Rpl38
Rps25
Rpl7l1
Rps10
Rpl23
Rpl18
Rpl12
Rps7
Rpl4
Rplp2
Rpl27
Rps13
Rps8
Rpl24
Time (h)
Chaperonin-containing T complex
Tcp1
Cct7
Cct2
Cct4
Cct3
Cct8
Cct5
RNA polymerase II
Polr2a
Polr2l
Polr2e
Polr2b
g
Annotated physical interactions within proteins with rhythmic synthesis
Whole-cell
PPI enrichment p=0.3
Complexes
PPI enrichment p=4.78e-05
Average node degree
h
AHA incorporation (native PAGE)
Time (h) 24 30 36 42 48 54 60 66
kDa
Strep-HRP
245
190
135
Total protein (SDS-PAGE)
Ponceau
245
135
100
AHA incorporation (au)
n=3, p=0.02
Time (h)

FIGURE 4

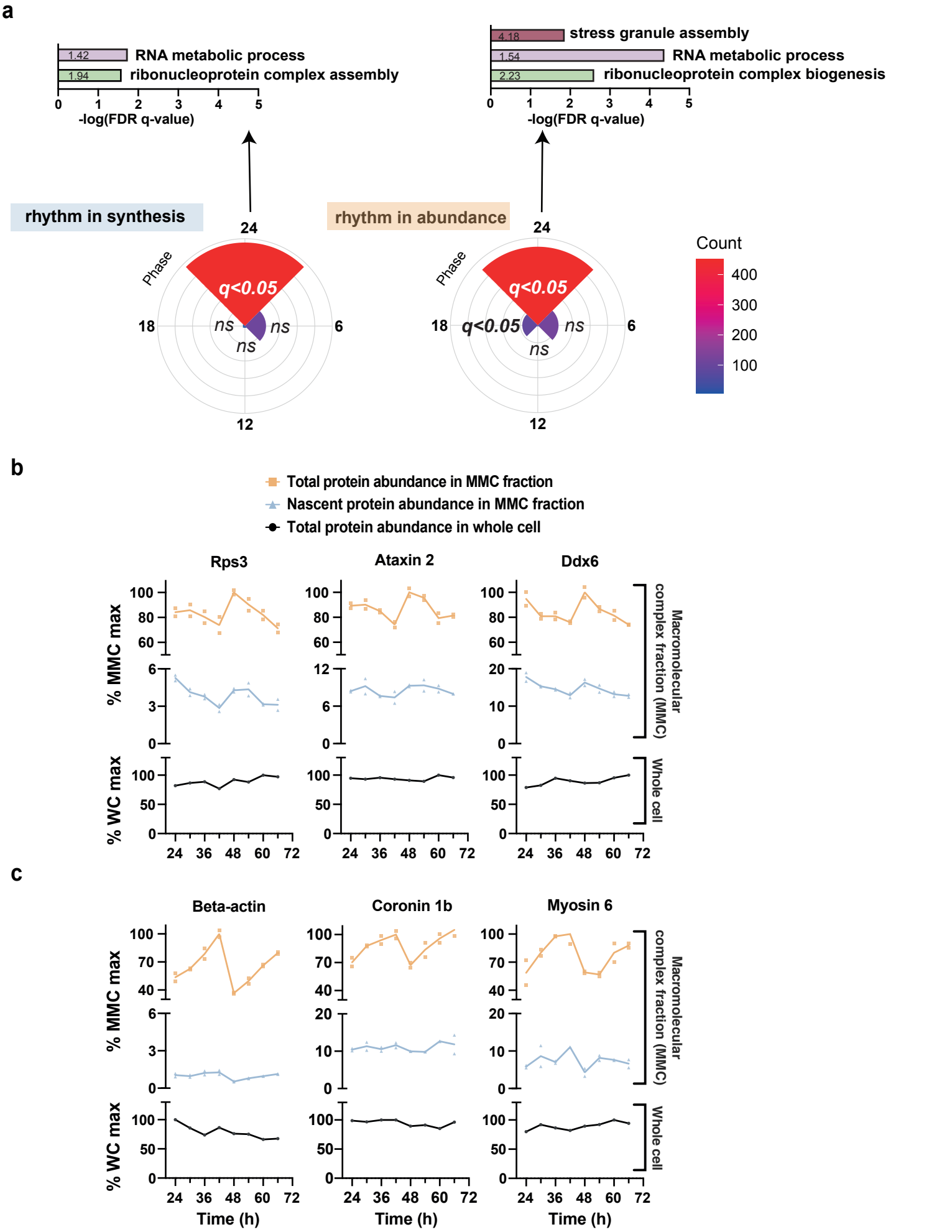
a
1.42
RNA metabolic process
1.94
ribonucleoprotein complex assembly
-log(FDR q-value)
4.18
stress granule assembly
1.54
RNA metabolic process
2.23
ribonucleoprotein complex biogenesis
-log(FDR q-value)
rhythm in synthesis
rhythm in abundance
Phase
q<0.05
ns
Count
400
300
200
100
b
Total protein abundance in MMC fraction
Nascent protein abundance in MMC fraction
Total protein abundance in whole cell
Rps3
Ataxin 2
Ddx6
% MMC max
% WC max
Macromolecular complex fraction (MMC)
Whole cell
c
Beta-actin
Coronin 1b
Myosin 6
Time (h)

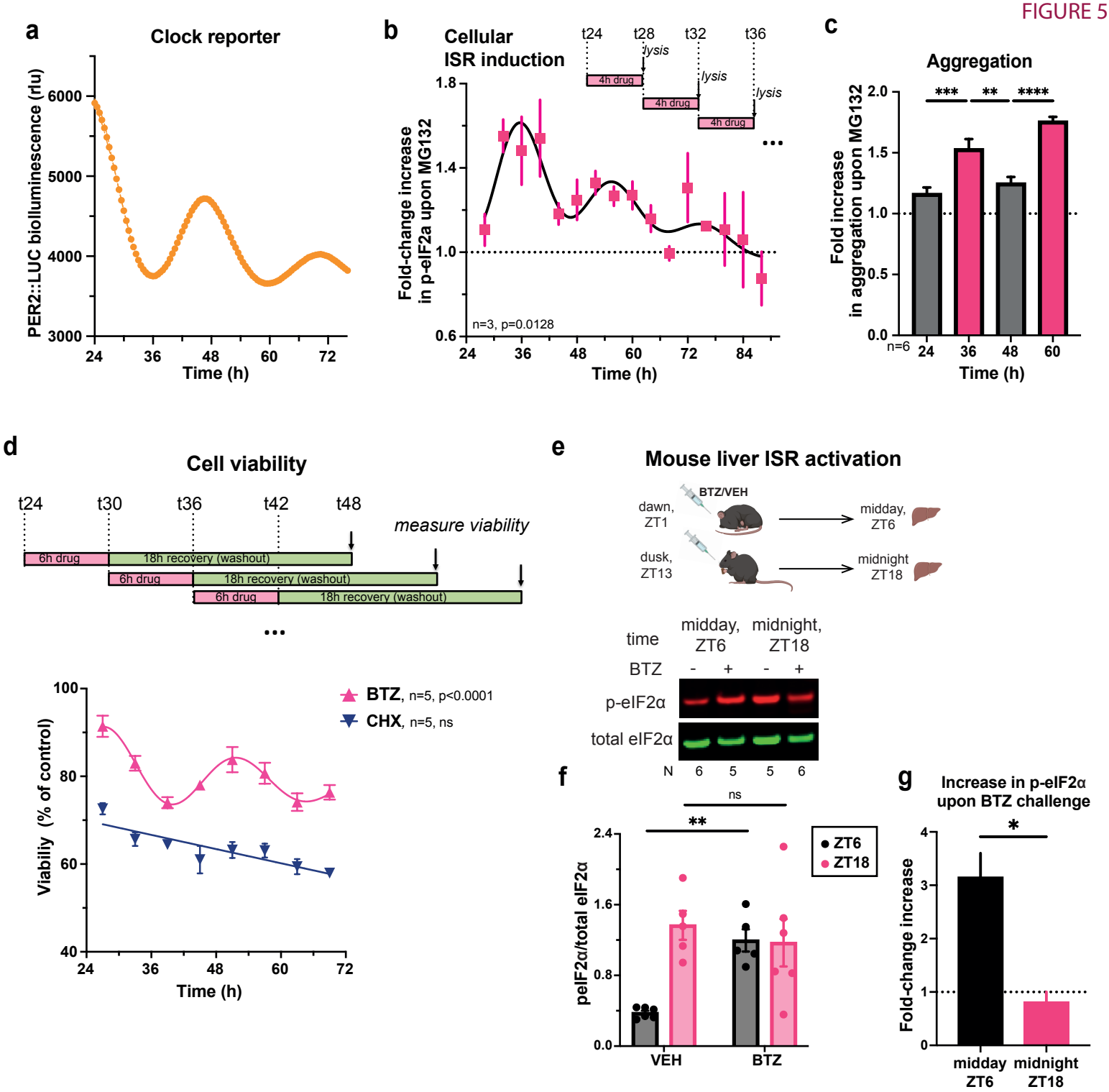
a
Clock reporter
PER2::LUC bioluminescence (rlu)
6000
5000
4000
3000
24
36
48
60
72
Time (h)
b
Cellular ISR induction
t24
t28
t32
t36
lysis
4h drug
Fold-change increase in p-eIF2a upon MG132
1.8
1.4
1.0
0.6
n=3, p=0.0128
84
Time (h)
c
Aggregation
Fold increase in aggregation upon MG132
2.0
1.5
1.0
0.5
0.0
***
**
****
n=6
Time (h)
d
Cell viability
t24
t30
t36
t42
t48
measure viability
6h drug
18h recovery (washout)
Viability (% of control)
100
80
60
40
BTZ, n=5, p<0.0001
CHX, n=5, ns
Time (h)
e
Mouse liver ISR activation
BTZ/VEH
dawn, ZT1
dusk, ZT13
midday, ZT6
midnight ZT18
time
midday, ZT6
midnight, ZT18
BTZ
p-eIF2α
total eIF2α
N
6
5
5
6
f
ns
**
peIF2α/total eIF2α
2.4
1.6
0.8
0.0
ZT6
ZT18
VEH
BTZ
g
Increase in p-eIF2α upon BTZ challenge
*
Fold-change increase
4
3
2
1
0
midday ZT6
midnight ZT18